Cranfield University

Jeffery Raymont

Electrode Optimisation for Piezoelectric MEMS Transfer Bonded Devices

SCHOOL OF APPLIED SCIENCES

MRes
Thesis

Cranfield University

SCHOOL OF APPLIED SCIENCES

MRes
Thesis

September 2008

Jeffery Raymont

Electrode Optimisation for Piezoelectric MEMS Transfer Bonded Devices

Supervisor: Dr. P.B. Kirby

Academic Year 2007 to 2008

This thesis is submitted in partial fulfilment of the requirements for the degree of Master of Research

© Cranfield University, 2008. All rights reserved. No part of this publication may be reproduced without the written permission of the copyright holder.

ABSTRACT

Optimisation can be viewed in many ways including that which is new and improvements to the materials, or methods that are already in place. Therefore we can define the two specific areas that make up the investigation relating to this work; those pertaining to new materials which may improve performance, and an analysis of the methods, and results, with regard to adhesion of the dissimilar materials incumbent in the present structures.

In this work, two candidate materials have been identified in order to improve the performance of the electrode structures present in MEMS devices used for piezoelectric applications. These are the conductive oxides, Lanthanum Nickel Oxide and Ruthenium Oxide, which have shown considerable promise because of their reported improvements in fatigue properties with PZT applications. They have been investigated as potential top layer electrodes as the literature has indicated that substantive improvements can be made in piezoelectric performance when conductive oxides are used as a top electrode.

The results for LNO as a top electrode using deposition through CSD yielded no crystalline presence when examined with XRD. However, the results indicate a possible amorphous presence when subjected to a strict cleaning regime and crystallisation using rapid thermal annealing. LNO deposition through CSD, when used as a top electrode with PZT has not been previously reported. This warrants further investigation as a basis for future work.

Conductive ruthenium oxide has been deposited through sputtering using a ruthenium target source and an 80/20 argon/oxygen mix. The results for ruthenium oxide deposited on to glass slides indicate that resistivity improves with annealing temperature. The results indicate successful ruthenium deposition on to PZT 30/70 but have produced mixed results when subjected to annealing because of the thickness of the ruthenium oxide deposited.

Two methods for measuring adhesion have been evaluated for their suitability in relation to thin metal films. The multi pass wear scratch test proved unsuitable for producing meaningful results with films deposited on to PZT. The pull test produced some results which mean that comparative analyses are possible for the thin film systems making up the electrode structure.

The stressed overlayer technique has been used as a means to evaluate the work of fracture for the metal electrodes making up the present structure. A model has been used on the blister structures resulting from the stressed overlayer. In addition, the method has enabled qualitative judgments of the electrode structures submitted for analysis.

Keywords:
PZT, Adhesion, Pull Testing, Conductive Oxides, LNO, RuO_2, Stressed Overlayer

ACKNOWLEDGEMENTS

I would like to thank my supervisor, Dr P.B. Kirby for his guidance through the project.

I would also like to thank Dr. D. Bhattacharyya for his assistance in the clean room and performing numerous XRD sessions. In addition, my thanks go to Mr R. Wright for his help with the stressed overlayer and Mr. P. Gkotsis for his help with sputtering.

I would also like to express my gratitude to Mr. K. Lawson for supplying the pull tester and ruthenium target and Mr J. Rao for the ruthenium oxide's subsequent deposition.

Finally, I must thank Mr M. Kershaw for the XPS analysis and Mr A. Dyer for performing the Scratch Test.

TABLE OF CONTENTS

TABLE OF FIGURES vii
TABLE OF TABLES..... viii
TABLE OF EQUATIONS ix
1 Introduction..... 1
1.1 Micro Electro Mechanical Systems (MEMS) 1
1.2 Batch integration of high quality materials for microsystems (Q2M for short) 1
1.3 Materials, Effect and Function 2
1.3.1 The Present Stack 2
1.3.2 Piezoelectric Effect 3
1.3.3 Lead Zirconate Titanate (PZT) 3
1.4 Areas of investigation 3
1.4.1 Conductive oxides 4
1.4.2 Ruthenium Oxide 4
1.4.3 Lanthanum Nickel Oxide (LNO) 4
1.4.4 Summary of conductive oxides 4
1.4.5 Measurement methods for Adhesion 5
1.4.5.1 Tape Test 5
1.4.5.2 Pull Test..... 5
1.4.5.3 Peel Test 6
1.4.5.4 Scratch testing with a nanoindenter. 6
1.4.5.5 Summary of measurement methods 7
1.4.6 Stressed Overlayer 7
1.5 Summary of introduction 7
2 Literature Review and Background 8
2.1 The In-situ bottom electrode structure..... 8
2.1.1 Platinum and Titanium..... 8
2.1.2 Bottom Electrode Summary 9
2.2 The In-situ Top electrode..... 9
2.3 Ferroelectric Materials..... 9
2.3.1 Critical properties of ferroelectric materials 9
2.3.2 Lead Zirconate Titanate (PZT)..... 10
2.4 Fabrication 12
2.4.1 Sputtering 12
2.4.2 Thermal evaporation 13
2.4.3 The Chemical Solution Deposition (CSD) technique..... 13
2.5 The Effects of Processing 13
2.5.1 Effects of stress on thin films 13
2.5.2 Intrinsic stress from deposition 14
2.5.3 Extrinsic stress from processing dissimilar materials..... 15
2.5.4 Effects of CSD processing 15
2.5.5 Reliability of PZT structures 16
2.6 Conductive Oxides 16
2.6.1 LNO 16
2.6.2 Ruthenium Oxide..... 16
2.7 Adhesion Energy 17
2.8 Stressed Overlayer..... 17

2.8.1 Stressed overlayer materials 17
2.8.2 Stressed overlayer analysis methods 18
3 Sample Preparation 20
3.1 Bottom Electrode Preparation 20
3.1.1 Titanium/Platinum Deposition 20
3.1.2 X-Ray Diffraction (XRD) Analysis 20
3.1.3 XRD after Titanium/Platinum Deposition 21
3.2 PZT Deposition 21
3.2.1 PZT 30/70 Deposition 22
3.2.2 PZT 52/48 Deposition 22
3.3 Top Electrode Deposition 23
3.3.1 Platinum 23
3.3.2 Chrome/Gold 23
3.4 Sample Preparation Summary 24
4 Results and Analysis Section 25
4.1 Analysis of in-situ materials 25
4.1.1 Growth stress of titanium platinum electrode 25
4.1.2 XPS of Titanium/platinum electrode with PZT deposition and etch-back. 26
4.1.3 Depth Profile of Ti/Pt after PZT deposition and etch-back 27
4.1.4 Summary in-situ materials Analysis 28
4.2 Lanthanum Nickel Oxide (LNO) 29
4.2.1 Processing Parameters for LNO 29
4.2.2 LNO Trials 29
4.2.2.1 LNO Trial One 29
4.2.2.2 LNO Trial Two 30
4.2.2.3 LNO Trial Three 31
4.2.2.4 LNO Trial Four 32
4.2.2.5 LNO Trial Five 33
4.2.2.6 Summary of LNO trials 34
4.3 Ruthenium Oxide 35
4.3.1 RuO_2 Deposition 35
4.3.2 RuO_2 Analysis 36
4.3.2.1 Analysis of RuO_2 deposited on Glass slides 36
4.3.2.2 Analysis of RuO_2 deposited on PZT 30/70 38
4.3.2.3 Resistivity Measurements for Ruthenium Oxide 41
4.3.2.4 Summary of Ruthenium Oxide activity 42
4.4 Adhesion Methods 42
4.4.1 Pull Test 43
4.4.1.1 Sample Preparation 43
4.4.1.2 Pull Test Results 44
4.4.1.3 Summary of pull test method 44
4.4.2 Scratch test 45
4.5 Stressed Overlayer 46
4.5.1 Stressed Overlayer Sputtering parameters 46
4.5.2 Stress Measurements for stressed overlayer 47
4.5.3 Qualitative Results of Stressed Overlayer 48
4.5.4 Blister Analysis 50

4.5.5 Work of Fracture 51
4.5.6 Summary of Stressed Overlayer 53
5 Conclusions 54
5.1 Conductive Oxides 54
5.2 The in-situ bottom electrode 55
5.3 Adhesion Methods and their Results 55
5.4 Stressed Overlayer 56
5.5 Summary of Conclusions 57
5.6 Further Work 57
REFERENCES 59
Appendices 63
Appendix A 64
Appendix B 65

TABLE OF FIGURES

Figure 1-1 The Present Stack 2
Figure 2-1 Characteristic ferroelectric hysteresis 10
Figure 2-2 Unit cell of Tetragonal PZT 11
Figure 2-3 Effect of temperature and composition on PZT 11
Figure 2-4 Effects of stress on the film-substrate system 14
Figure 3-1 Linear plot of XRD for Si/SiO_2/Ti/Pt 21
Figure 3-2 XRD PZT 30/70........ 22
Figure 3-3 XRD after PZT 52/48 deposition........ 23
Figure 4-1 Mounting arrangement of wafer for Dektak 25
Figure 4-2 XPS of Ti/Pt after PZT removal 27
Figure 4-3 Depth Profile of Ti/Pt after PZT deposition and etch-back 28
Figure 4-4 XRD LNO Trial One 30
Figure 4-5 XRD LNO Trial Two 30
Figure 4-6 XRD LNO on Si/SiO_2/Ti/Pt/PZT 30/70........ 31
Figure 4-7 XRD Trial 3 LNO on Si/SiO_2/Ti/Pt/PZT 30/70 1 hour 32
Figure 4-8 LNO Trial 4 XRD LNO on Pt/PZT 70/30 32
Figure 4-9 LNO Trial 5 XRD LNO PZT 30/70 RTA 500°C 33
Figure 4-10 LNO Trial 5 XRD LNO PZT 30/70 RTA 600°C 34
Figure 4-11 Representative Sample of LNO surface conditions. 34
Figure 4-12 XRD of RuO_2 on glass slide 36
Figure 4-13 Sample 1 RuO_2 on Glass Slide annealed at 450°C 37
Figure 4-14 Sample 2 RuO_2 on Glass Slide annealed at 550°C. 37
Figure 4-15 XRD Analysis (Linear version) of RuO_2 deposited on PZT 30/70 38
Figure 4-16 XRD Analysis (Logarithmic version) of RuO_2 deposited on PZT 30/70 ... 39
Figure 4-17 XRD Analysis (Linear version) of RuO_2 deposited on PZT 30/70 after annealing at 450°C for thirty minutes. 39
Figure 4-18 XRD Analysis (Logarithmic version) of RuO_2 deposited on PZT 30/70 after annealing at 450°C 40
Figure 4-19 Image of surface of RuO_2 deposited on PZT 30/70 after annealing at 450°C 40
Figure 4-20 XRD Analysis (Logarithmic version) of RuO_2 deposited on PZT 30/70 after annealing at 550°C 41
Figure 4-21 Test specimen ready for pull test 43
Figure 4-22 Multiple pass wear scratch test on Platinum contacts........ 45
Figure 4-23 Platinum peeling after stressed overlayer 49
Figure 4-24 Blister formation from 906nm Stressed Overlayer deposition on /Ti/Pt/PZT 30/70 with Etch-back........ 49
Figure 4-25 Processed Ti/Pt with blisters and telephone chord-like Formation 50
Figure 4-26 Image of circular blister with microscope and Dektak 50
Figure 4-27 Scan profile of Blister from Dektak........ 51
Figure A1 Graph of Chrome/Gold Voltage/Current Measurements 65
Figure A2 Effect of Annealing at 450°C on V/I Relationship 66
Figure A3 Effect of Annealing at 550°C on V/I Relationship 67

TABLE OF TABLES

Table 4-1 Ruthenium Oxide processing.. 35
Table 4-2 Pull Test results... 44
Table 4-3 δ values of samples before the Stressed Overlayer test................................ 47
Table 4-4 Values for stress related parameters in Stressed Overlayer (SO) application 48
Table A1 Peak Comparer and Percentage Quantities.. 64
Table A2 Four point probe measurements for Chrome/Gold Reference....................... 65
Table A3 Four Point Probe Measurements for Ruthenium Oxide on Glass Slides........ 66

TABLE OF EQUATIONS

Equation 4-1 Stoney Equation.. 26
Equation 4-3 Stoney One Dimensional Beam Model... 48
Equation 4-4 Critical buckling stress σ_b.. 51
Equation 4-5 Residual stress of the buckle film σ_r 52
Equation 4-6 Interfacial fracture energy $\Gamma(\Psi)$.. 52

1 Introduction

The introductory section introduces the necessary technology areas, materials, methods and subject areas that are the background to the work described herein.

1.1 Micro Electro Mechanical Systems (MEMS)

In definition, Microsystems Technology (MST), or Micro Electro Mechanical Systems (MEMS) refer to the same technology. Where a device combines a mechanical function and electrical activity, and is fabricated at the micron scale, thus forming an autonomous system that has some intelligence. So a function (say a sensor) will act on a stimulus, producing a result that is communicated in a form ready for use.

The advantages of integration, in sensor applications, are that small scale changes (that otherwise may be lost) can be processed in-situ. Also, it avoids any randomness that can result from a function being detached from its processing. So, there is potential for more accurate and repeatable results.

The main reason for the rapid development of MEMS technology is that the fabrication technology is already in place, in the well developed form of silicon processing in the microelectronics industry. Thus, there are mature processes in place for the bulk production of small, individual devices, at a (competitive) cost effective price.

The specific processes for producing MEMS differ from those used in the standard semiconductor industry. In that they use silicon for its mechanical properties, producing shapes and three dimensional structures for a particular application.

Current applications using MEMS technology include hard disk drives, inkjet printers, pressure transducers, accelerometers (airbags), gyroscopes (guidance), optical switches (data transmission and visual displays) and micro mirror arrays (projection displays). Other applications include chemical and biological sensors and microfluidic devices for chemical analyses.

The transfer bonding alluded to in the title of this thesis, is the product of the Q2M partnership and concerns batch integration of materials. A brief section summarising the work, and principles, is given below.

1.2 Batch integration of high quality materials for microsystems (Q2M for short)

The Q2M project [http://q2m.4m-net.org/Q2M_Home] is EU FP6 sponsored and sets out a core mission to develop bonding technologies that combine high quality materials and components so that batch-wise integration can be used whilst maintaining the economies of full wafer processing of the constituent parts. So, an individual element

can be processed to its ideal conclusion without any compromise dictated by any incompatible material and process.

One of Cranfield's activities as part of this project concerns the development of piezoelectric actuation of Radio Frequency MEMS (RFMEMS) switches (which can then be transfer bonded into a silicon circuit). This, invariably, requires sandwiching a functional material with conducting electrodes and thus introduces the problems, and adhesion issues, associated with bonding dissimilar materials.

In our case the 'microdevice distribution' principle means that the electrode and PZT stack making up the functional element can be optimised and produced with the economies of a full scale wafer production. Then it can be selectively transferred, and adhesive bonded, to a receiving wafer with CMOS compatibility. Thus, the cost of device production can be shared over the number of wafers populated.(Guerre et al., 2007), (Guerre et al., 2008)The Q2M bonding process adds another activity that causes potential adhesion problems, as it requires a sustained temperature of 400°C for an hour.

1.3 Materials, Effect and Function

This section introduces the various materials and their function as part of the focus of this work. The aim is to briefly cover the subject material that is relevant to the project. It is not exhaustive but serves as an introductory text.

1.3.1 The Present Stack

The present stack is shown below as Figure 1-1, and consists of a silicon wafer substrate, followed by silicon dioxide, titanium, platinum, PZT and the top electrode, which is presently platinum. Formerly, the top electrode structure has been made up by the bi-material combination of chromium and gold.

Figure 1-1 The Present Stack

Platinum
PZT
Platinum
Titanium
Silicon Dioxide
Silicon

The present stack uses various metals to provide the conducting electrodes. They are used in consort, to add virtues not available from their individual properties. In the

present structure the bottom electrode is comprised of the bi-material pairing of titanium and platinum. The titanium is used as an adhesion layer because it bonds well and platinum interfaces well with the PZT, and does not readily oxidise. The stack is completed with platinum as a top electrode to make the system symmetric.

The process in place is refined to produce high quality piezoelectric devices but there is a reliability problem, particularly with the adhesion of metals to PZT. Unfortunately, a lot of the present evidence is anecdotal in that there is a known problem but there is no quantitative analysis of the metal contact's adhesion to PZT. In addition, there is limited study of the effects caused by PZT and its deposition.

1.3.2 Piezoelectric Effect

The piezoelectric effect was first discovered by the Curie brothers (Pierre and Paul-Jacque), finding that an external force applied to particular crystals generated a charge on the surface. It is an effect that is naturally occurring in quartz. The effect relies on a crystal structure that is non-centro-symmetric and thus an applied stress causes a strain in the material and the ion movement resulting from the deformation causes a change in charge.(Madou, 1997)

The direct piezoelectric effect is where a stress causes a material deformation and produces a voltage. To picture the effect, an example is readily available in the form of a stylus over a record. Here, the grooves of the vinyl form the stress on the stylus that is transduced into an electrical signal and amplified for music reproduction. The converse piezoelectric effect being the opposite in that a voltage will produce a stress in the material and change its shape.

1.3.3 Lead Zirconate Titanate (PZT)

The functional material used in the present structure is Lead Zirconate Titanate (PZT) which is a solid solution of lead titanate and lead zirconate. It is a ferroelectric material of perovskite structure (ABX_3), and the intrinsic atomic structure is the basis of the material's properties in that it has the inherent offset non-centro-symetric arrangement required for piezoelectric performance.

PZT has attracted considerable interest because of its superior performance virtues as a piezoelectric material. The applications for piezoelectric PZT include sensors, actuators, transducers and resonators.

1.4 Areas of investigation

This sub section introduces the various materials and fields of endeavour that make up the research.

1.4.1 Conductive oxides

A particularly active area in the last few years is in the field of conductive oxides. This is a promising avenue for this project because of the potential for matching the PZT structure and forming a well matched interface. In addition, conductive oxides offer the potential for a fully chemical bond with PZT, avoiding the problems associated with the adhesion of dissimilar materials where bonding between layers does not readily occur.

One of the potential causes of degradation in performance with PZT is thought to stem from oxygen vacancies causing dead layers close to the electrode. One of the advantages of using conductive oxides is that they are believed to rectify the oxygen deficiency built-up at the interface by providing a source of oxygen from the electrode itself. Consequently, there is a resulting improvement in the fatigue characteristics associated with ferroelectric performance.

1.4.2 Ruthenium Oxide

One material ripe for inclusion as part of this project is ruthenium oxide, as there is a deposition source available in the form of a ruthenium target that can be used in conjunction with sputtering.

Ruthenium oxide has a rutile structure and reports suggest that fatigue properties in PZT have been improved with its use as an electrode. The benefits are attributed to a reduction in oxygen vacancies mentioned above but, in addition it provides a diffusion barrier preventing the inter-diffusion of lead and oxygen which are often present in the search for perovskite PZT.(Izyumskaya et al., 2007)

1.4.3 Lanthanum Nickel Oxide (LNO)

Another much studied conductive oxide material in collaboration with PZT is Lanthanum Nickel Oxide (LNO). Again its inclusion as a candidate material is partially based on the availability of a source, in the form of a sol for CSD.

LNO has a perovskite structure, like PZT, and has a similar lattice parameter. LNO has more promising polarisation fatigue prevention characteristics in comparison with platinum, because of oxygen vacancy sinking properties. In interfacing with PZT, perovskite LNO has the inherent advantages of a well matched structure and chemistry.(Izyumskaya et al., 2007)

1.4.4 Summary of conductive oxides

There are two promising non-standard candidate materials available for investigation, LNO and ruthenium oxide. Both show promising performance characteristics, certainly

in relation to the fatigue and ageing mechanisms associated with piezoelectric performance of PZT.

1.4.5 Measurement methods for Adhesion

Part of the scope of this work is an analysis of the potential methods available to make practical measurements for adhesion. Subsequently, the methods available need to be examined to evaluate their suitability with thin films based on silicon substrates.

There are four main methods used for practical measurements of adhesion and these are explained in the section below.

1.4.5.1 Tape Test

The tape test is subject to an international standard ASTM D3359 -08 entitled Standard Test Methods for Measuring Adhesion by Tape Test. The basic procedure for which is the affixing of a pressure-sensitive tape to the area under test and its subsequent removal with forces as normal to the surface as is practicable. The tape involved is important for measurement consistency.

The tape test is a quick and easy examination of minimum adhesion requirements. It is qualitative in nature as it indicates a simple pass, or fail condition. If the coating, or film, survives the test then it is deemed to pass. No more than that can be gleaned from the test. It would be best applied as the most basic part of a tiered structure of testing methods. Some adaptation of the tape test is possible with the use of different strengths of adhesive.

1.4.5.2 Pull Test

The pull test uses an applied normal force to test the failure at the weakest point in the structure. The test is applied by affixing a test stud to the surface under test and the test stud being subject to a normal force by pulling. Obviously this is a test of the weakest interface in the hierarchy so the adhesive used to affix the test stud to the sample has to be stronger than the bond tested.(Mittal, 1976)

In dealing with silicon wafer samples the underside of the test specimen also requires adhesion to a test plate to avoid wafer fracture. Also, the size of the test head dictates a minimum size for samples, so any cleaved samples require affixing to a base that is larger than the test head. The pull test is destructive in nature but can produce quantifiable results, and is certainly capable of qualitative judgement based ranking of the samples subject to testing.

1.4.5.3 Peel Test

Again this test is destructive in nature and it shares the same methods as those highlighted above but the test is applied differently. The test requires a test stud to be affixed to the sample and, as the name implies, the test is based on the force required to peel the film off of the substrate. However, as the film is peeling, it is stretched, so it is subject to plastic deformation. Hence, the limitations of the test are that the values measured are not just adhesion measurements but have an added element that is the product of the ductility of the material as it undergoes plastic deformation.(Kim et al., 1989)

As a method the peel test is only quantitative with the same materials undergoing the test. Otherwise, at best, it is qualitative in that it reveals whether a material combination passes the test for a given load. In conclusion, with the variety of materials involved in the scope of this work it would be unsuitable as a method.

1.4.5.4 Scratch testing with a nanoindenter.

Scratch testing relies on the repetitive motion of a diamond stylus, at constant speed, over the surface of the material under test, introducing stresses between the surface layer and substrate. Generally, in operation the diamond stylus is static and provides a normal load to the sample under test, which is displaced in a perpendicular direction on a vibrating stage. The test is destructive and the results obtained are in terms of the smallest load causing failure.

The influences on measuring the critical load for failure include both intrinsic and extrinsic parameters. The intrinsic parameters of the test include scratching rate, loading rate and those properties related to the diamond, which are radius and wear. Of these, the only non-reproducible factor in the test method, over a period of time, is the effect of wear on the stylus. However, the rate of wear on the stylus, over a group of samples is not prohibitive to reliable and reproducible results. (Steinmann et al., 1987)

The extrinsic parameters affecting the test are substrate hardness, coating thickness and roughness of the substrate and electrode materials. In addition, there are the contributions from friction. For the materials under investigation most of these properties are the same, or similar. Using the same stylus means that the only variable is the coefficient of friction which would be different between metals and conductive oxides.(Steinmann et al., 1987)

The Nanotest 600 system at Cranfield has two loading heads providing differing forces. The micro loading head provides forces between 0.1N and 20N and the nano loading head provides forces in the range of 10μN to 500mN. The scanning (scratch testing) module is destructive but determines the failure at the interface.

There are two modes of operation within the nanotest 600 scanning module. These are ramped load scratch testing and multi-pass sub-critical load scratch testing.

The ramped load scratch test examines the film failure at a critical normal load which is revealed by a depth change. In addition this can provide a qualitative ranking of the adhesion of samples with different coatings.(Impey, 2007-2008)

Multi-pass sub-critical load scratch testing uses repeated scratches over the same wear track and can reveal the mechanical fatigue behaviour, the cohesive failure associated with fracture and the adhesive failure associated with delamination.(Impey, 2007-2008)

1.4.5.5 Summary of measurement methods

The methods for direct measurement of adhesion have been introduced. The methods available for the project are the tape test, the pull test and the scratch test using a nanoindenter. The peel test is not available, but as has been pointed out previously, it would not be suitable for the range of materials envisaged in the scope of this work.

Whether the methods available are suitable for thin films deposited on to silicon based substrates is yet to be proven. As no measurements for adhesion have been attempted part of this work is an evaluation of the methods as well as experimental results.

1.4.6 Stressed Overlayer

The main problem in measuring adhesion arises from the method influencing what is being measured. So, whilst repeatable and comparative what is being measured is not a true value for adhesion. One method to overcome these shortfalls and get a truer measure of the work of adhesion is the stressed overlayer, or superlayer, method. The basic premise of which is the application of a secondary film overcoat that has sufficient elastic energy, through the strain allied with deposition and film thickness, to cause the underlying material to delaminate.

The stressed overlayer approach works because a uniform stress is applied to the film/substrate system under test and any plasticity is confined out-of-plane. The basic assumptions in using the method are that the superlayer and film/Substrate do not react and that the interface is not compromised by the test.(Bagchi et al., 1994)

1.5 Summary of introduction

Background to the work has been provided for the materials in use and their effect and function. The aims of the project have been analysed with the introduction of suitable candidate materials in the shape of the conductive oxides LNO and ruthenium oxide. Additionally, methods for the direct measurement of adhesion have been described and the stressed overlayer technique has been introduced for evaluating a truer value for the work of adhesion.

2 Literature Review and Background

This section examines the background and literature relating to the project work. They are entwined because of the nature of the material relating to the project. It serves as an extension to the introductory section, in that it explores the background in a more focused fashion. Further, there are sections dealing with the specific requirements of the project.

2.1 The In-situ bottom electrode structure

The bottom electrode structure serves a dual purpose in PZT structures in that is not only necessary as a conductive electrode but also serves to seed the growth of the PZT. Importantly, the PZT's ferroelectric performance is directly related to its surface morphology, microstructure and crystal structure. Therefore, the bottom electrode is inherently important to the structural development of a high quality crystalline result.

The important qualities for the bottom electrode are that it is epitaxial and either singly crystalline, or in orientation. In addition, it should have a similar lattice parameter and structure to that of PZT. Also, the electrode must be impervious to PZT's constituents so that interdiffusion does not occur during growth. This is also true for the relationship between the electrode and substrate.(Izyumskaya, 2007b)

2.1.1 Platinum and Titanium

The positive virtues of platinum as an electrode with PZT are that it does not readily form an oxide and has a similar lattice parameter to PZT which is inherently preferable for crystal nucleation. In addition, it is supposedly a good barrier against lead diffusion.(Izyumskaya, 2007b) In addition, Nam et al. (Nam et al., 2000) report that platinum makes a good electrode because of its low leakage current as well as high thermal conductivity.

Titanium has better bond forming abilities than platinum so it makes for a good adhesion layer to silicon dioxide.(Franssila, 2004) However, titanium forms an (insulating) oxide readily so it would be entirely unsuitable as a conductive interface with PZT. Even when used as an adhesion layer, the thickness of the titanium layer has to be controlled because it is known to diffuse through platinum with the thermal cycling caused by the PZT CSD process. The results of interdiffusion are numerous, including titanium hillock formation and the possibility of shorting the electrode and the potential of forming titanium oxide at the boundary with the PZT.(Izyumskaya, 2007b)

Aside from titanium's use as an adhesion layer, in conjunction with platinum, it also provides a diffusion barrier to the underlying silicon dioxide. Otherwise, with the advent of high temperature annealing there is the possibility of platinum silicides being formed.(Izyumskaya, 2007b)

There are reports that when titanium is used as an adhesion layer with platinum there is a problem caused by diffusion of the titanium during processing. Particularly with any processing that involves thermal changes. The result of this thermal impact on the diffusion of the titanium is that it can give rise to hillock formation. These hillocks form to relieve the compressive stress from the platinum deposition by RF magnetron sputtering. This formation of titanium hillocks is particularly problematic in capacitive applications and also has implications for the general reliability of MEMS devices using this bi-layer pairing.(Nam et al., 2000)

2.1.2 Bottom Electrode Summary

Platinum has a very similar lattice parameter to PZT and does not form a stable oxide, which is why it continues to be popular as a bottom electrode for PZT. Hence, with platinum's seeding properties assured it seems prudent to concentrate on the top electrode performance in relation to any new materials.

2.2 The In-situ Top electrode

Platinum is currently in use as a top electrode material. However, it does not have the clear cut advantages that it has as a bottom electrode material, particularly in terms of PZT nucleation. For instance platinum, on its own has a known catalytic effect particularly in a hydrogen environment and this causes degradation on the characteristics of ferroelectric thin films.(Yuh et al., 2002)

Sama et al. (Sama et al., 2008) conclude that when platinum is used as a top electrode material it has a deleterious effect on the dielectric, piezoelectric and ferroelectric of PZT.

2.3 Ferroelectric Materials

Ferroelectric materials are a branch of functional materials that have attracted considerable interest because of their superior performance virtues. They are characterised by a specific, and critical, set of properties. Once the criteria for ferroelectric materials are met, this special class of materials exhibits pyroelectric, piezoelectric and dielectric properties. However, the functional performance of ferroelectric materials is directly related to correct processing.

2.3.1 Critical properties of ferroelectric materials

Ferroelectric materials are polar, and their electrical polarisation is reoriented by spontaneous dipole movement under the application of an electric field. This is possible because of an extrinsic property associated with domains and their behaviour.

The ferroelectric material consists of domains where the dipoles are self aligned. Under the application of a poling electric field these domains change, the dipoles within them change and with wall movement and dipole alignment, they switch to form a high energy fully polarised system that is termed, metastable. When the applied field reaches a saturation point (P_s) there is effectively one aligned domain. On reversing the applied field a characteristic hysteresis forms and results in a remanent polarisation (P_r) which holds the residual changes. The polarisation then reduces until the coercive field strength (E_c) is reached. Further field application thereafter starts switching the polarisation.(Izyumskaya, 2007a) The characteristic hysteresis for a ferroelectric material is shown below as Figure 2-1.

Figure 2-1 Characteristic ferroelectric hysteresis

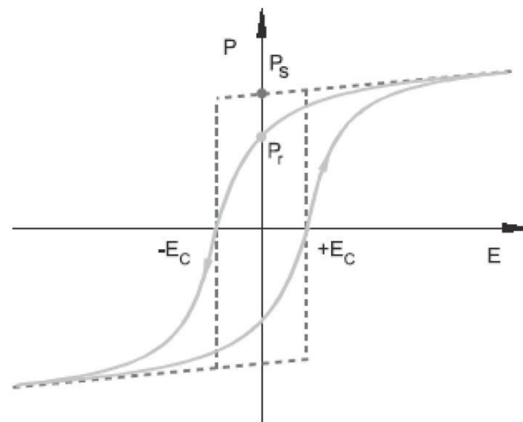

Diagram from Ferroelectrics: Functional Materials : Dr R Dorey; Ferroelectrics PZT 29th October-2nd November 2007 lecture notes, SAS, Cranfield University.

The potential applications for functional materials exhibiting ferroelectric behaviour are those requiring dielectric, piezoelectric and pyroelectric properties. The dielectric property gives rise to capacitive applications such as a camera flash. The application of poling gives rise to the piezoelectric effect with applications in sensors, actuators, transducers and resonators.

The inherent property of spontaneous polarisation together with poling, subsequent saturisation and its reversal gives rise to pyroelectric properties and potential applications with thermal imaging and motion detectors. Finally, as the ferroelectric material has two possible states, together with remanence, there are potential applications as a material for non-volatile RAM.

2.3.2 Lead Zirconate Titanate (PZT)

PZT is the functional material at the heart of this work so it is necessary to cover the subject material in some detail. This begins with the atomic arrangement which is the basis of the material's properties. Figure 2-2 below, shows the unit cell for tetragonal PZT with the heavy, and lower valency, lead atoms taking the corners of the cube and the oxygen atoms taking face centre positions. The higher valency titanium and

zirconium atoms form the offset non-centro-symetric tetragonal structure.(Izyumskaya, 2007a)

Figure 2-2 Unit cell of Tetragonal PZT

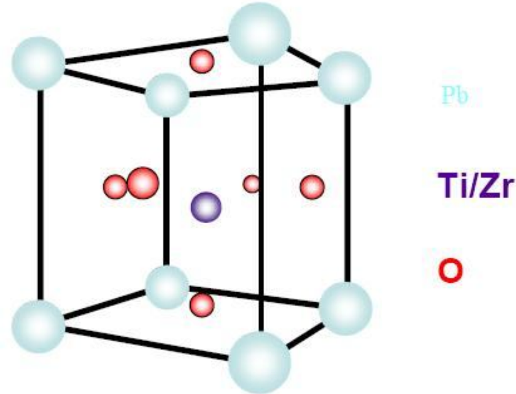

Diagram from Ferroelectrics PZT: Functional Materials : Dr R Dorey; Ferroelectrics PZT 29th October-2nd November 2007 lecture notes, SAS, Cranfield University.

PZT is a solid solution of lead titanate and lead zirconate. It is a ferroelectric material of perovskite structure (ABX_3), and has an intrinsic atomic property that when tetragonal or rhombohedral in crystal geometry exhibits spontaneous polarisation. Thus, it has at least two orientation states without an applied electric field. This is possible providing that the temperature is below the Curie temperature T_c, otherwise the material will be cubic and the material will not exhibit ferroelectric properties. The variation of crystal geometry with temperature and composition is shown below as Figure 2-3.(Izyumskaya, 2007a)

Figure 2-3 Effect of temperature and composition on PZT

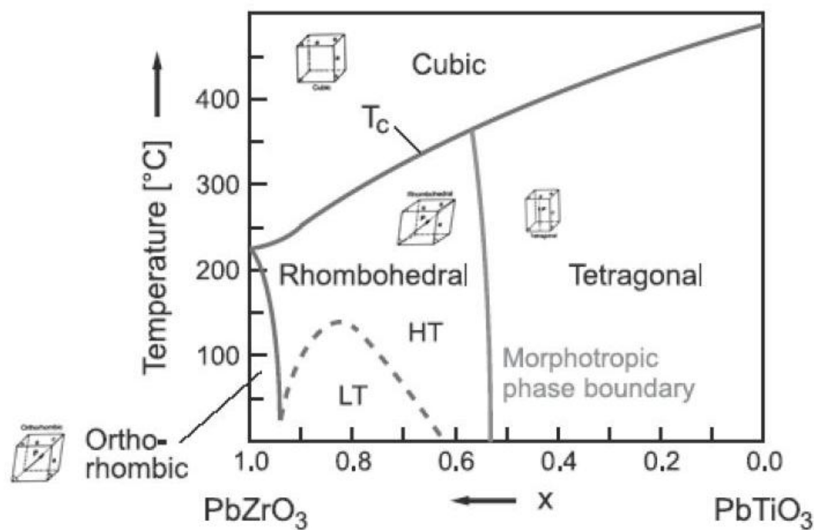

Diagram from Ferroelectrics PZT: Functional Materials: Dr R Dorey; 29th October-2nd November 2007 lecture notes, SAS, Cranfield University.

Here, x indicates the compositional variation of zirconium and titanium content in $PbZr_xTi_{1-x}O_3$. This variation in x gives rise to specific properties of the PZT, with titanium rich tetragonal, and zirconium rich rhombohedral, variants possible. The dividing line is termed the morphotic phase boundary. Compositions at this boundary produce exemplary piezoelectric and ferroelectric performance. More recent work suggests that another phase is present in this area; the monoclinic phase.(Izyumskaya, 2007a)

Recent applications using PZT and the piezoelectric effect include ultrasonic motors, probes for atomic force microscopy, cantilever actuators and medical applications with ultrasonic transducers (Wilson et al., 2007a).

2.4 Fabrication

There are three deposition methods available within the department, sputtering, thermal evaporation and the sol-gel chemical solution deposition (CSD) route. The CSD method offers the advantages of exact compositional control, highly pure products and is kinder to the environment than other deposition methods. It is appealing in terms of cost but requires refinement in terms of the fabrication process used thereafter. Whereas, sputtering requires a target which may be expensive but offers deposited materials of good quality.

2.4.1 Sputtering

Sputtering is a plasma technique where ion bombardment is used to hit a target and release atomic material that, in turn, additively deposits a thin film of target material on the substrate. The gaseous plasma is generated in a low pressure, high vacuum environment, typically with an, inert, argon gas supply. The energy feed for the plasma coming from an RF or DC power source.(Freund and Suresh, 2003b)

The variants on offer for Physical Vapour Deposition, or sputtering, are DC, RF or RF magnetron. DC is used for metals and offers high deposition rates, whereas RF is generally used with a DC bias and offers the potential for the deposition of insulating films. The Magnetron confines the electrons in the plasma and the twofold benefits of this are; maximum energy of ion bombardment because there are no electron collisions to reduce the energy and with the electrons contained there is more probability of further ionisation.(Freund and Suresh, 2003b)

When sputtering a hybrid electrode structure consisting of an adhesion layer and top electrode layer, like titanium and platinum, the deposition follows directly without breaking vacuum. Thus the cleanliness of the interface is assured, which is a major factor to promote adhesion.(Franssila, 2004)

2.4.2 Thermal evaporation

Thermal evaporation is a simple technique where the source material required for deposition is resistively heated on a tungsten element in a vacuum and the hot atoms deposit onto the substrate.

2.4.3 The Chemical Solution Deposition (CSD) technique

The process for Chemical Solution Deposition (CSD) of PZT begins with the preparation of the sol, which is synthesised from a lead precursor and titanium/zirconium alkoxide complex together with an organic solvent to promote adhesion whilst spin coating.

Once the PZT complex is synthesised the deposition process involves a layer-by-layer approach. Each layer is spin-coated, pyrolised to drive off the solvent and then crystallised. The process being repeated until the desired thickness is achieved.

2.5 The Effects of Processing

As films become thinner the effects of any stresses are exacerbated. The thin films under investigation in this study concern electrodes generally in the 100nm range, but also concern bi-material electrodes with 8nm components. This means that there is considerable scope for the full panoply of stress related problems through weakened layers to possible adhesion problems and on to complete delamination failure through the effects of processing alone. The areas of concern are those issues related to the deposition of the thin film itself and the effects of further processing on dissimilar materials with differing characteristics.

2.5.1 Effects of stress on thin films

The two different types of stresses are compressive and tensile. The effects wrought on the film-substrate system can be pictured through the simple diagrams included below as Figure 2-4. These diagrams show the film-substrate system accommodating the result of the stresses.

Figure 2-4 Effects of stress on the film-substrate system

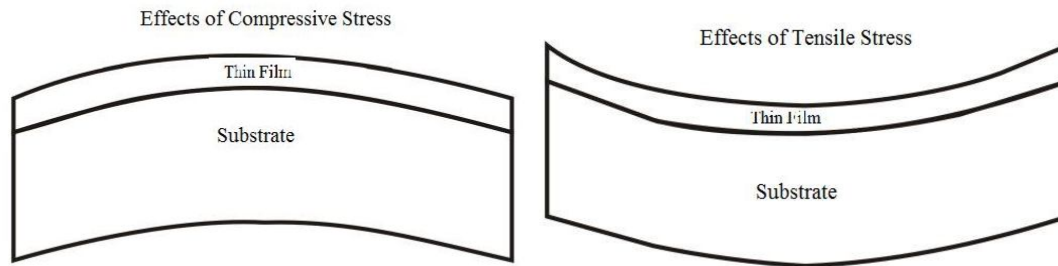

The worst case scenario resulting from stresses in the thin film system can be delamination. In this case there is sufficient energy stored in stress to overcome the adhesion energy of the thin-film to substrate bond.

2.5.2 Intrinsic stress from deposition

Intrinsic or, more appropriately, growth stresses are those concerned with the materials deposited, together with the method, and temperature, of deposition and its associated environment.(Freund and Suresh, 2003a)

The standard methods for depositing metallic thin films are physical vapour deposition methods including sputtering and thermal evaporation. The processes share the common requirement of a low pressure, high vacuum environment. This gives rise to a thermodynamic situation where the deposited materials are inelastic and not in equilibrium. Hence, there is low atomic mobility and any strain from the process will be frozen in to the materials.(Gerberich and Cordill, 2006)

Sputtering can be prone to contamination and specific mechanisms for stress are involved because of the use of a gas generated plasma Firstly, there is the possibility of gas absorption causing a strain which is generally avoided by biasing the substrate. Additionally, there is the potential for atomic peening form ion bombardment, in which the high energy ions impinge on areas outside of the interstitial sites. All of these factors generally give rise to a compressive stress in sputtered films, although this is not true for all materials. In contrast, the situation with thermal evaporation is the reverse as this generally produces tensile stress in the films.(Freund and Suresh, 2003a)

As an example of growth stress, the current practice when using platinum as a top electrode is the use of annealing to improve adhesion. So, in addition to the other effects of processing, the platinum appears to be in compressive stress as a result of deposition.

2.5.3 Extrinsic stress from processing dissimilar materials

The extrinsic stresses are those that occur to the film after growth. Thus, they are those stresses associated with the influence of extraneous physical factors, such as temperature, either through further processing or as a result of operating conditions.(Freund and Suresh, 2003a)

The main cause of extrinsic stress between adhered dissimilar materials is that caused by the mismatch in their respective coefficients of expansion. So, any subsequent processing that produces a thermal cycle will mean a disparity between the expansion of the materials whilst heating and their subsequent contraction whilst cooling. Hence, there will be a change in the stresses between the films before and after processing.(Freund and Suresh, 2003a)

2.5.4 Effects of CSD processing

The present processing situation is that the lower electrode combination has to survive the PZT deposition, which is built up by successive layers of spin coated sol which are pyrolised at 300-400°C to drive off the solvents added to promote PZT adhesion. The method revolves around several thin layers being deposited to prevent the PZT layer cracking, which is a problem when thick (100nm+) layers are deposited. Once the desired thickness of PZT has been achieved, the chemical solution deposition (CSD) route requires post annealing at 600-700°C to crystallise the PZT film.

The PZT stoichiometry has to be precise, in terms of growth and nucleation, to achieve the perovskite phase. This is to avoid pyroclore and fluorite phases nucleating. Unfortunately the PbO-ZrO_2-TiO_2 system making up PZT gives rise to a couple of problems which directly relate to adhesion. For the perovskite phase to form lead concentration has to be precise. Insufficiency in the lead content can lead to pyrochlore formation, however in excess lead content, the formation of secondary phases of lead oxide can occur. This gives rise to a problem when lead ions or PbO molecules are not incorporated into the PZT perovskite lattice, as they can be highly diffusing and volatile above 500°C, which is below the crystallisation temperature for PZT. This, potentially, exacerbates the adhesion problem of metals to the PZT.(Muralt, 2000)

Gkotsis et al.(Gkotsis et al., 2007) in their processing of the $Si/SiO_2/Ti/Pt/PZT/Ti/Au$ stack have noted the effects of repetitive thermal cycling on the bottom electrode structure whilst processing PZT by CSD. By using wafer curvature techniques for analysis, before and after deposition of a bi-layer titanium/platinum bottom electrode together with the same method after PZT deposition and its subsequent removal, a picture builds up of the effects of this processing on the bottom electrode structure. The results find that the sputtered titanium, platinum electrode system is compressive after deposition. However, the effects of thermal cycling with ten layers of PZT, on top of titanium and platinum, with differing coefficients of expansion, means that the bottom electrode system becomes tensile. In fact, it becomes as tensile after PZT deposition as it was compressive beforehand.

2.5.5 Reliability of PZT structures

Once the full stack has been processed there are other processes and issues which have an impact on the device electrodes and their adhesion. The first issue concerns the necessity of poling PZT, so that it functions as a ferroelectric material. In this process a high field strength is applied to the electrode at an elevated temperature, which can produce enough strain to delaminate the electrode. Also, there is possible delamination in-service, as a result of ageing processes causing fatigue and depolarisation. The piezoelectric ageing process stems from the hi-energy poled domains reverting to a more energetically favourable condition. This results in a reduction of the piezoelectric coefficients and gives rise to the depolarised, fatigued, condition.(Wilson et al., 2007b)

2.6 Conductive Oxides

The original motivation for research into the use of conductive oxides was the noted polarisation fatigue effects when platinum was used as an electrode in capacitive applications. The indications are that conductive oxides have better fatigue properties than platinum because they reduce the oxygen built up at the interface. The other noted benefits in their use are those of compatibility with PZT. These include their similarities structurally, chemically and in lattice terms.(Izyumskaya et al., 2007)

2.6.1 LNO

The top electrode selection plays an important part in device functionality. Recent reports indicate that when comparing the performance of LNO and Pt as a top electrode the LNO top electrode reduces the coercive field (positive and negative), there is a slight increase in remnant polarisation and in addition, maximum polarisation increases by 20%. In addition, there is significant improvement in electromechanical properties with LNO as a top electrode. (Sama et al., 2008)

Kim et al.(Kim and Lee, 2002) use deposition by RF magnetron sputtering to fabricate LNO as a top electrode in their investigations into the effects of polarisation fatigue caused by annealing in an environment containing hydrogen. They find that LNO has definite advantages over platinum with its known catalytic effect.

N. Sama et al.(Sama et al., 2008) report that when LNO is used a top electrode it seems to dominate electrical properties. Whatever stack is used the permittivity increases whenever LNO is used as a top electrode. However, the top layer LNO electrode was deposited using sputtering.

2.6.2 Ruthenium Oxide

Although the benefits associated with fatigue properties have been reported for ruthenium oxide. There are particular problems with its use as a bottom electrode as it

has been noted that PZT was polycrystalline because nucleation was more difficult, which results in lower remanent polarisation.(Izyumskaya et al., 2007)

Lee et al. (Lee et al., 2005) report the use of ruthenium oxide as a top electrode material for RF MEMS applications. Using PZT as a functional material for piezoelectric actuation in ohmic contact switches they report excellent RF performance. In addition, they find operation can be conducted at low voltages, and therefore with lower consumption, making them suitable for mobile and wireless applications.

LNO and ruthenium oxide have both been used successfully as top electrodes with PZT in piezoelectric applications. Further, reports indicate that platinum may have a negative impact on piezoelectric performance when used as a top electrode. So, in addition to the ageing and fatigue effects mentioned in the introduction, it seems that conductive oxides may offer benefits in performance when used as top electrodes in piezoelectric applications with PZT.

2.7 Adhesion Energy

The various methods for direct adhesion measurements mentioned in the introduction are generally qualitative in nature. They also suffer from the same problem in that they colour the results obtained because of the methods of test application. Also, adhesion has been applied in a general sense. In fact, it has a specific meaning in terms of the surface energies of the film and substrate system and the energy required to separate them. The principle being that it takes energy to create a surface and therefore it takes more energy to separate them, as this creates two surfaces. (Moody et al., 2007)

Hence, whilst the qualitative methods mentioned previously have merit in relative terms what they are able to measure is not the true work of adhesion. Thus, in order to get a quantitative measure of adhesion, various methods have been devised. One of which is the stressed overlayer, which forces delamination and then uses a model on the resulting structure of the blisters and buckles produced to get a value for the adhesion energy.

2.8 Stressed Overlayer

Pioneered by Bagchi and Evans(Bagchi et al., 1994), with their work on copper and dielectrics, the stressed overlayer, or superlayer, technique serves as a method for the measurement of fracture at the film surface interface. It uses a secondary layer as an overcoat to the surface and interface under examination. The basic premise being that the stressed overlayer has sufficient elastic energy through its thickness and residual stress that it causes delamination at the film/surface interface.

2.8.1 Stressed overlayer materials

The film/substrate materials that have been the subject of investigation using the stressed overlayer technique are mainly those materials of direct concern to the semiconductor and MEMS industries. The materials investigated with the stressed

overlayer method include gold and chrome/gold on sapphire substrates, titanium on silicon (100), Copper on silicon dioxide, silicon nitride and polyimide, titanium on silicon (100) and platinum on silicon dioxide. (Moody et al., 2000)(Kinbara et al., 1998)(Bagchi and Evans, 1996)(Lee et al., 2004)

The materials used to induce delamination as the film of application using the stressed overlayer technique include tantalum nitride, nickel, chromium, molybdenum, molybdenum chromium and tungsten. (Moody et al., 2000) (Kinbara et al., 1998)(Bagchi and Evans, 1996)(Lee et al., 2004)(Modi and Sitaraman, 2004)(Cordill et al., 2007)

The advantage in using a stressed overlayer film is that the deposition methods are often the same as the films forming the interface under test. So, the film and stressed overlayer share the same growth stresses. In addition, the methods of deposition are standard fabrication technologies and therefore commonly available.(Modi and Sitaraman, 2004) Also, the stressed overlayer can be deposited without breaking vacuum with more assurance that it will adhere to the surface under test. In addition, variation in film thickness can be controlled by the time taken for deposition and, of course, the process can be easily characterised by simple experimentation

2.8.2 Stressed overlayer analysis methods

The results of using a stressed overlayer give rise to a plethora of techniques and models for their analysis. They are also used in conjunction with other methods such as nanoindentation. One example of this uses a molybdenum stressed overlayer with an indent in the film to store some stress beneath the overlayer. In this method the stresses are calculated using radius of curvature measurements and the circular blister resulting is measured using atomic force microscopy (AFM). The resulting measurements are then combined to give a measure of fracture based on a critical crack extension force model. (Lee et al., 2004)

The buckles and blisters can form in a spontaneous fashion in which case they do not require any other methods for inducement. The blister profile can be measured and the results can be subject to various models depending on the shape of blister. The particular shapes of interest are the telephone-chord types which tend to form to reduce strain energy in the system. These telephone chord structures can straighten and can then be effectively modelled using either a pinned circular model or a straight buckle model.(Cordill et al., 2007)

Whilst most applications of the stressed overlayer use compressive stress to produce buckles and blisters either for use in a suitable model or in collaboration with indentation techniques. There are other methods that use interfacial film peeling as a result of the concentration of tensile stress.

Zheng et al.(Zheng and Sitaraman, 2007) use a method of patterned strips under a titanium test layer to modify the stress driven by the deposited chromium stressed overlayer. The patterned strip, titanium sample and chrome are subject to a perpendicular cut through the centre of the sample with an etching process, which

selectively removes all but the patterned strip. Further etching removes the patterned strip and the energy held in the chromium stressed overlayer delaminates the titanium film. The delamination continues until the energy supplied by the stressed overlayer is insufficient to overcome the inherent fracture toughness of the film. Thus, the length of peel determines the films fracture toughness. In this method, results for the fracture toughness for 90nm of titanium are between $3.45J/m^2$ and $5.7J/m^2$.

3 Sample Preparation

This section is dedicated to sample preparation which when cleaved provided the specimens for investigation and analysis.

The format of the section is from the bottom up, as it is encountered in fabricating a complete device stack. The starting point is a (100) orientated silicon wafer 400µm thick with a thermally grown oxide layer of 200nm thickness. The SiO_2 layer has a twofold purpose in that it provides an insulating base and provides a barrier layer to promote high temperature stability for platinum based electrodes.

3.1 Bottom Electrode Preparation

The standard bottom electrode configuration is a bi-material electrode consisting of titanium and platinum. Before the deposition could take place the Si/SiO_2 wafer was subject to a cleaning process. This consisted of oxygen plasma cleaning using a barrel etcher at a pressure of 2mBar for three minutes, using a power of 14W.

3.1.1 Titanium/Platinum Deposition

The 8nm titanium adhesion layer was sputter deposited using an 8” x 4” rectangular 99.995% pure titanium target. The titanium was deposited at room temperature with RF sputtering using a Nordiko 2500 System with a base pressure of 5.7×10^{-7} Torr. The sputtering conditions were 300W with a D.C. bias of 1.5V using argon gas for the plasma with a flow rate of 40.4 SCCM under a sputtering pressure of 5.1mTorr (10mTorr with a sensor in a different location). The sputtering time was 24 Seconds.

Without breaking vacuum 100nm of platinum was deposited with a 99.999% pure, 8” x 4” platinum target using DC magnetron sputtering at a voltage of 440V and a current of 0.7A. The deposition rate for platinum at 0.7A is 2.05 nm per second, so the platinum deposition lasted 49 Seconds.

The first task is to characterise the deposition through X-Ray Diffraction (XRD) analysis.

3.1.2 X-Ray Diffraction (XRD) Analysis

This uses a monochromatic source of X-rays for incident radiation and the results are provided by detecting the diffracted results as the X-rays impinge on the crystal lattice of the sample surface.

All sample scans were conducted over the 20° to 60° range for 2θ analysis using a Siemens D5005 X-Ray Diffractometer using a copper source for X-Rays and the use of

a Goebbl mirror to intensify the beam and provide a monochromatic source. The software used was Diffrac-plus by Siemens.

3.1.3 XRD after Titanium/Platinum Deposition

The XRD analysis of titanium/platinum gives the basis for any future XRD analysis of later samples as the intense platinum peak can be determined on its own. It is shown below as Figure 3-11 below gives analysis in linear form.

Figure 3-1 Linear plot of XRD for Si/SiO_2/Ti/Pt

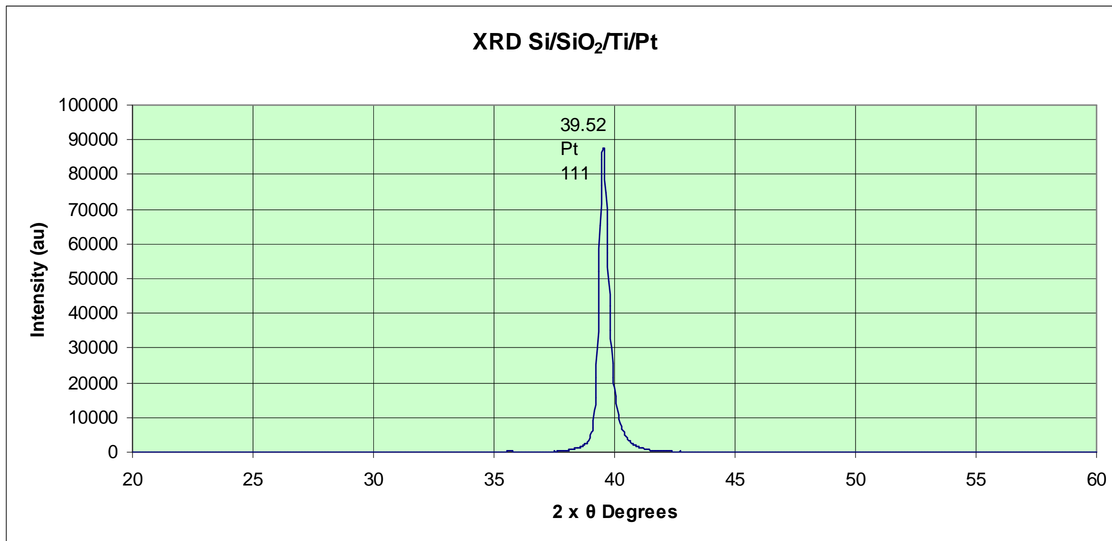

Here we can see the intense (111) peak for platinum at a value of 39.52° for 2θ.

As the bottom electrode system is now in place, it is possible to deposit our functional material, Lead Zirconate Titanate (PZT).

3.2 PZT Deposition

PZT deposition is through the CSD process. Where the required thickness of PZT is achieved through the application of successive layers of spin coated sol which is pyrolised to drive off solvents and then crystallised.

All spin coating was conducted in a clean room to avoid any contamination and dust. The deposition of the sol through spin coating used a syringe with a 0.2 µm inorganic filter and a Cookson G3-8 spin coater. The spin coating was conducted at 3000 RPM for thirty seconds, with two seconds for acceleration and one second for deceleration. As the process has been well characterised these spin conditions yield 50nm of PZT, per layer.

3.2.1 PZT 30/70 Deposition

The procedure for PZT 30/70 requires pyrolysis at 200 °C for 40 seconds, for each layer. The crystallisation temperature is 530 °C and requires seven minutes for the first layer, with five minutes per layer thereafter. Eight layers of PZT yield a total deposition of 600nm. The pyrolysis process used a Cimerec 3 hotplate and the crystallisation process used the Sawntec HP-160/700 system.

For reference in further analysis an XRD post PZT 30/70 deposition in logarithmic form is shown below as Figure 3.2.

Figure 3-2 XRD PZT 30/70

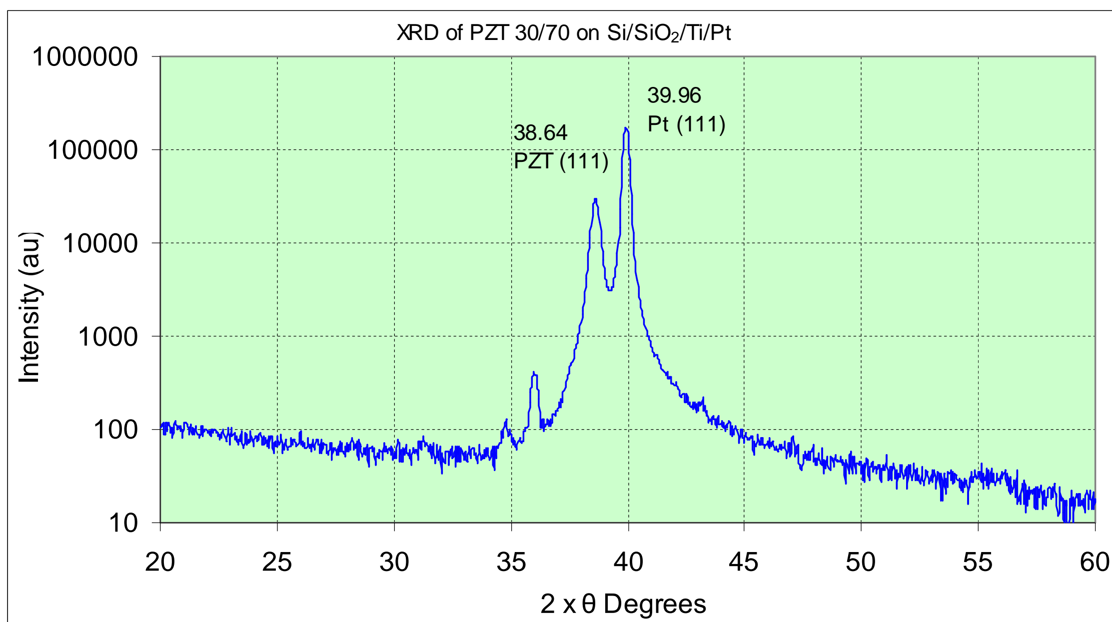

3.2.2 PZT 52/48 Deposition

PZT 52/48 was deposited using a 0.4M solution. The method is the same as outlined above, but there are variations in the temperatures and timings. Here, each layer is pyrolised at 350 °C for three minutes and crystallised at 580°C. Again, the first layer requires seven minutes for crystallisation and all subsequent layers required five minutes. Seven layers were deposited making a total thickness of 550nm. The pyrolysis process used a Cimerec 3 hotplate and the crystallisation process used the Sawntec HP-160/700 system

The base processing is complete so Figure 3-3 below gives the results of XRD analysis after the deposition of PZT 52/48 on $Si/SiO_2/Ti/Pt$.

Figure 3-3 XRD after PZT 52/48 deposition

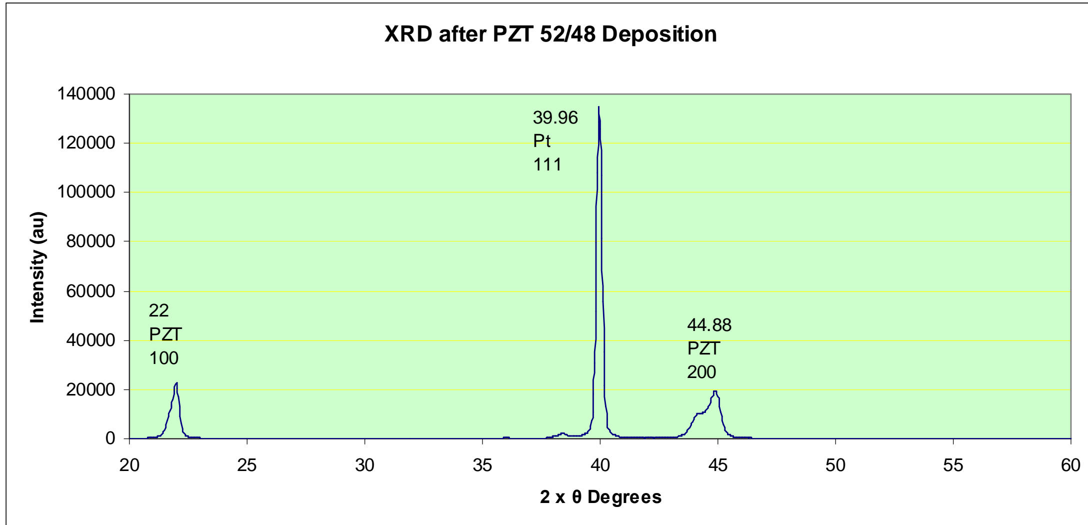

As the PZT has been deposited and characterised the standard in-situ process can be completed with the addition of the top electrode.

3.3 Top Electrode Deposition

Conventional metal based top electrode structures were fabricated on cleaved samples to provide specimens for the adhesion analysis and the superlayer process. For comparison two electrode types were deposited, platinum and chrome/gold.

3.3.1 Platinum

The standard top electrode of 100nm of platinum was deposited on samples up to and including both variants of PZT, 52/48 and 30/70, using the same machine (Nordiko) and sputtering parameters, as for the deposition of the bottom electrode, mentioned previously. Again, prior to sputtering the samples were cleaned with an oxygen plasma.

3.3.2 Chrome/Gold

In this bi-layer electrode system the chromium serves as an adhesion layer. The chromium/gold bi-layer top electrode was deposited using the Edwards E480 System, and thermal evaporation using a base pressure $8x10^{-7}$ Torr and a current of 20A A.C.; for 10.1 nm of Chrome deposition the approximate timing was 46 seconds and for 58.7nm of gold the timing is approximately 117 seconds. Again, the samples presented to the system were those up to, and including, PZT 52/48 and 30/70.

3.4 Sample Preparation Summary

This section explains the methods used to prepare the samples that when cleaved form the basis for the results and analysis section that follows. The samples with stacks up to, and including PZT, of 30/70 and 52/48 compositions, from the basis for investigations into conductive oxide deposition and analysis.

The samples for adhesion analysis and for the superlayer technique take samples cleaved at various stages through the cycle of preparation for the complete stack.

4 Results and Analysis Section

This results chapter is separated into five sections with the opening section containing analysis of the in-situ bottom electrode materials and the effects caused on them by growth stresses and the PZT deposition process.

The methods and results associated with the conductive oxides LNO and ruthenium oxide are dealt with in sections two and three, respectively. Thereafter, the penultimate section is dedicated to those results pertaining to adhesion methods and measurements. Finally, the chapter concludes with a section devoted to the use of a stressed overlayer technique and its results.

4.1 Analysis of in-situ materials

This section focuses on analysis of the bottom electrode system with titanium/platinum and includes calculation of the growth stresses from sputter deposition. Thereafter, there are two analyses of the material effects of the PZT CSD processing on the titanium/platinum electrode, through PZT deposition and etch-back. The first analysis pertains to the surface, and near surface, of the platinum and is conducted through X-Ray Photoelectron Spectroscopy (XPS) and the second analysis uses a depth profile to examine the structure of the complete titanium/platinum electrode.

4.1.1 Growth stress of titanium platinum electrode

The growth stress from titanium/platinum sputter deposition was determined by using the Stoney equation with radius of curvature measurements conducted with a Dektak 3 surface profiler. The Dektak surface profiler is equipped with a custom made sample stage to facilitate radius of curvature measurements. The mounting arrangement for wafers is shown below as Figure 4-1.

Figure 4-1 Mounting arrangement of wafer for Dektak

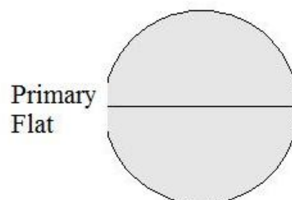

Once the wafer is in place the scan is conducted along the centre of the wafer for a distance of 5cm giving a scan radius of 25mm where the delta value is recorded at the

midpoint, which effectively models the cap on a sphere. The experiment is conducted on the Si/SiO_2 wafer and then repeated after the titanium/platinum electrode deposition.

The value of curvature obtained for Si/SiO_2 wafer was recorded as $4x10^8$µm and that recorded after titanium/platinum deposition was -5.3 $x10^7$µm with the negative value indicating that it is compressive.

The standard measurement method for stress are developments of those originally conceived by Stoney(Stoney, 1909) with his work modelling the effects of film deposition on beams and the resulting bending that this deposition causes. Using this method with wafer curvature measurements presupposes that the thickness of the film under investigation is far less than the underlying substrate and that the resulting deformation is extremely small.(Freund and Suresh, 2003c) When this is the case, the stress of the film σ_f, can be calculated using;

Equation 4-1 Stoney Equation

$$\sigma_f = \frac{E_s}{6(1-\nu_s)}\left(\frac{1}{R}-\frac{1}{R_0}\right)\frac{t_s^2}{t_f}$$

Where E_s, υ_s and t_s are the elastic modulus, the Poisson's ratio and thickness of the substrate, respectively; t_f is the film thickness and R_0 and R are respectively, the radius of curvature of the substrate before deposition, and after.

And substituting values E_s= 168GPa, υ_s =0.065, t_f = 0.108 x 10^{-6}m, t_s=400.2x10^{-6}m,
R = -5.3 x 10^7µm= -53m and R_0= 4 x10^8µm = 400m

Gives a value of σ_f = -0.95 GPa, or 950 MPa of compressive stress.

4.1.2 XPS of Titanium/platinum electrode with PZT deposition and etch-back.

All XPS analysis was conducted by Mathew Kershaw.

The sample presented for this test was $Si/SiO_2/Ti/Pt$; with PZT 52/48 deposited and then removed with Hydrofluoric acid (HF).

X-ray Photoelectron Spectroscopy (XPS) is a surface, or near surface analysis (to 10nm). It uses X-rays for a source and detects photoelectrons. Thus, the energy of the source is known and allied with that received at the detector it means that the difference in energy can be calibrated, and therefore identify a particular element from its characteristic energy levels.

Compositional analysis of the peaks and percentages of elemental quantities was performed by Mathew Kershaw and this has been included in Appendix A. It shows that

the specimen was composed of 1.9% lead and 32.9% platinum as well as the inevitable carbon and oxygen. The XPS of the Ti/Pt electrode with PZT and etch-back is shown below as Figure 4.2.

Figure 4-2 XPS of Ti/Pt after PZT removal

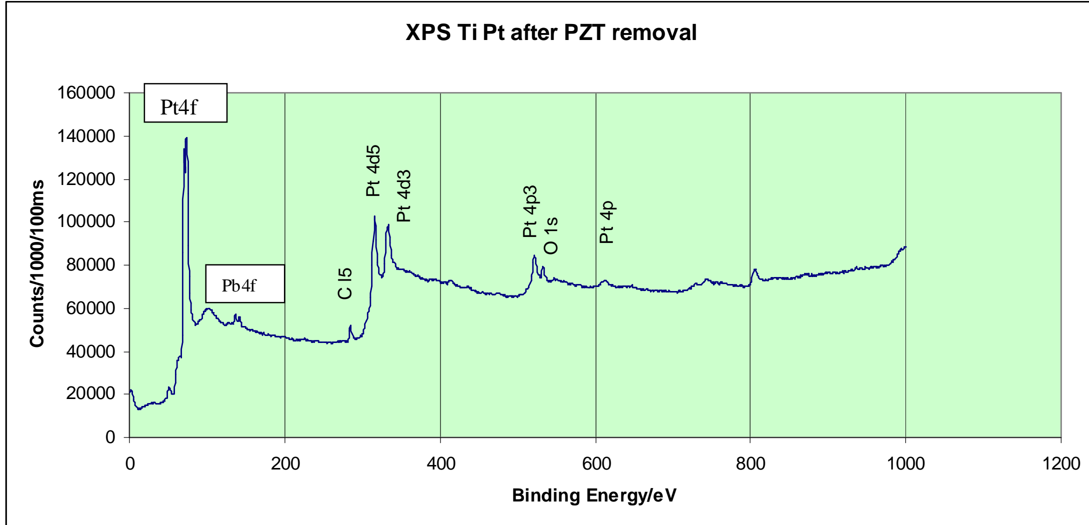

Allowing for the presence of carbon and oxygen that occurs with the inevitable exposure to air, the main thing to note is the lead presence. As the PZT was removed with HF then the oxides associated with PZT have also been removed. Hence, the lead presence is elemental and indicates that lead has migrated to the surface of the electrode or has partially diffused into the platinum's near surface. The effect would be to alter the electrode's performance and would have a deleterious effect on the adhesive qualities of the electrode. The one positive result from the analysis is the absence of titanium. So, the 8nm titanium/100nm platinum combination does not have hillocks that would short the electrode. Additionally, it is clear that the titanium does not diffuse to the platinum surface causing a dead oxide layer between the platinum and PZT.

4.1.3 Depth Profile of Ti/Pt after PZT deposition and etch-back

This analysis method uses an ion beam to burrow into the platinum/titanium electrode with XPS to provide compositional analysis as the depth progresses through the extent of the titanium/platinum electrode to the SiO_2 layer.

Figure 4-3 Depth Profile of Ti/Pt after PZT deposition and etch-back

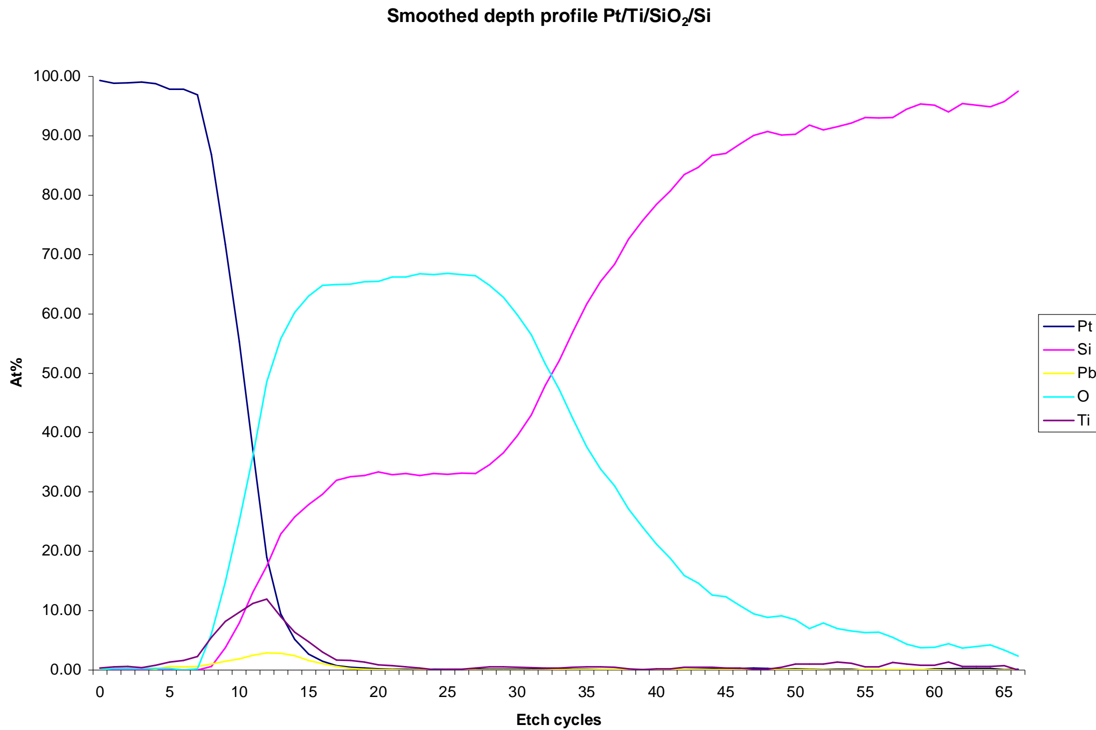

This analysis gives some indication of the material characterisation from the top of the platinum. Whilst not completely accurate there is some approximation of depth from the number of etches performed. The alarming fact is the presence of lead at some point into the platinum/titanium (looking top down) structure. Although, it is not intense and therefore probably less accurate as a result, it is yet more evidence of lead diffusion through the platinum.

The positive outcome is that the intensity of the titanium peak is strong where the platinum is weakening and the silicon and oxygen are strengthening indicating that it has not migrated far into the platinum. However, it does give some indication that there is more of a titanium/platinum solid solution at the base of the electrode, rather than separate layers.

4.1.4 Summary in-situ materials Analysis

The titanium/platinum electrode has significant residual compressive stress from sputter deposition. Unfortunately, as the sample was required for experimentation further analysis was not possible. The full impact on the titanium/platinum electrode system is not through its growth stresses alone but is only revealed after PZT processing and etch-back. However, as the literature cited in section 2.5.4 concerning the effects of CSD processing is directly related with the same materials it is possible to approximate that the tensile stress induced would be around the 900MPa figure. This is one of the significant factors in the deterioration of the adhesive qualities of the lower electrode system.

The direct analysis through XPS and the depth profiling show the alarming presence of lead. There are indications of the interdiffusion of lead into the platinum electrode which has another deleterious effect on the adhesive qualities of the electrode system. In addition, the adhesive qualities of the titanium/platinum electrode system face further erosion because of the partial diffusion of titanium into the platinum. Thus, there is evidence of a solid solution of titanium/platinum rather than discrete layers.

The one positive benefit highlighted through the analysis is that with an 8nm thickness of titanium there are no tangible signs of hillock formation.

4.2 Lanthanum Nickel Oxide (LNO)

The LNO sol available for the following trials was 0.1M in concentration and synthesised from citrus precursors using the Pechini method. It was prepared in 2005 by Dr Qi Zang.

4.2.1 Processing Parameters for LNO

In all of the LNO experimentation the spin coating was conducted at 3000 RPM for thirty seconds, with two seconds for acceleration and one second for deceleration. As was the case with PZT, all spin coating was conducted in a clean room to avoid any contamination and dust. The deposition of the sol through spin coating used a syringe with a 0.2 μm inorganic filter and a Cookson G3-8 spin coater.

In experimenting with LNO as a top layer electrode the first requirement is the characteristic crystallographic analysis brought by XRD to examine the structure of LNO on the completed substrate. So each trial is accompanied with its associated XRD analysis in linear form as the LNO intensity is likely to be weak at best. Miyazaki et al. (Miyazaki et al., 2004) report XRD peaks at values around 23° and 47° for (100) and (200) orientations, respectively.

4.2.2 LNO Trials

The method of deposition and spin parameters remained the same so each trial is distinguished by the methods adopted for cleaning and the changes in times and temperatures for pyrolisation and crystallisation.

4.2.2.1 LNO Trial One

Trial 1 was conducted with three layers of LNO deposited on top of PZT 30/70 with pyrolisation for five minutes at a temperature of 350°C. Crystallisation was conducted

for 31 minutes at a temperature of 650 °C in an air ambient atmosphere by leaving the lid up on the Sawntec heating system.

Figure 4-4 XRD LNO Trial One

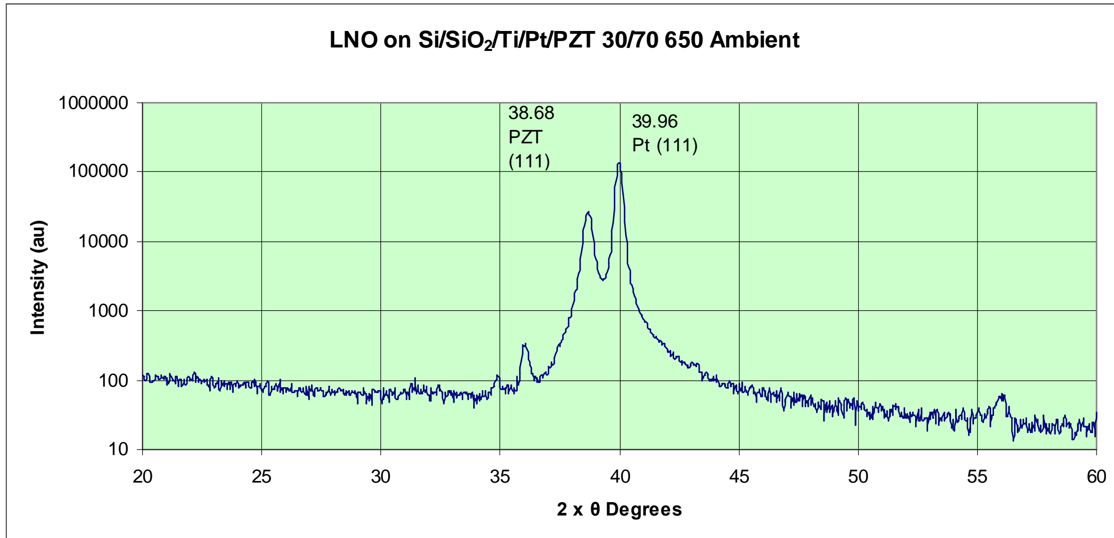

The XRD in logarithmic form shown above as Figure 4-4 indicates that there is no crystallographic evidence of LNO.

4.2.2.2 LNO Trial Two

Trial 2 was conducted with three layers of LNO deposited on top of PZT 30/70 with pyrolisation for five minutes at a temperature of 350°C. Crystallisation was conducted for 30 minutes at a temperature of 600 °C in an air ambient atmosphere by leaving the lid up on the Sawntec heating system.

Figure 4-5 XRD LNO Trial Two

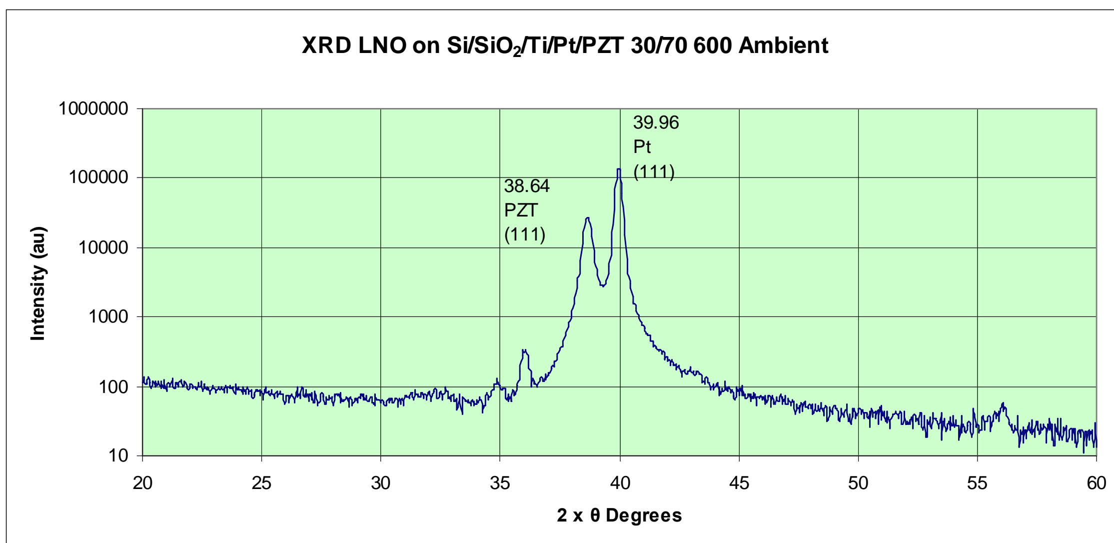

Again, Figure 4-5 showing the XRD in logarithmic form shows that there is no crystallographic evidence of LNO.

4.2.2.3 LNO Trial Three

Trial 3 was conducted with four layers of LNO deposited on top of PZT 30/70 with pyrolisation for two minutes at a temperature of 350°C. Crystallisation was conducted for 30 minutes at a temperature of 700°C although not with an air ambient atmosphere.

Figure 4-6 XRD LNO on Si/SiO_2/Ti/Pt/PZT 30/70

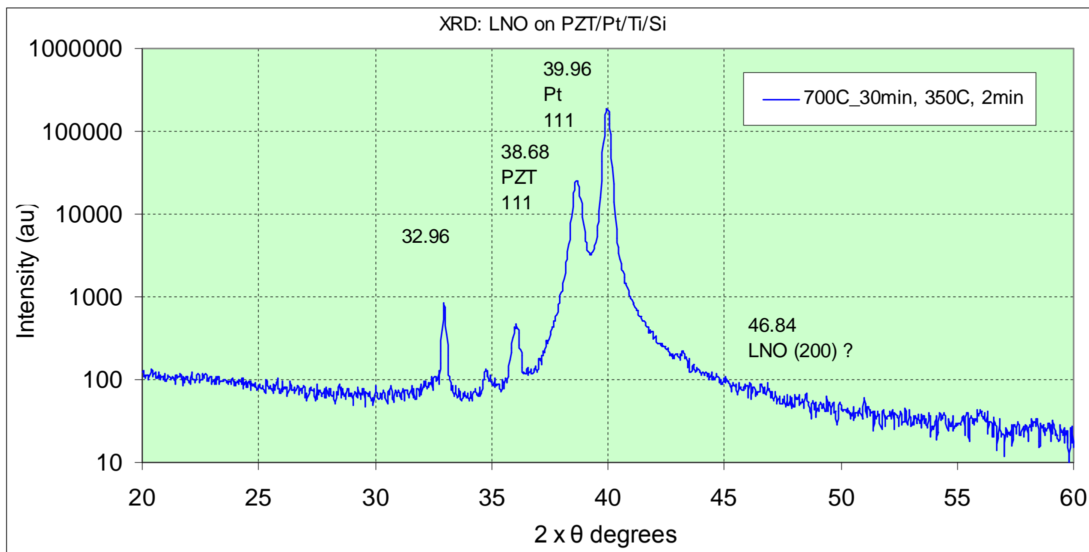

As the XRD shown above as Figure 4-6 gave an indication that there may be some life in the sample, crystallisation was conducted for a further half an hour. Thereafter the XRD analysis was repeated and is shown below as Figure 4-7 indicating that there was no positive change in the XRD characterisation.

Figure 4-7 XRD Trial 3 LNO on $Si/SiO_2/Ti/Pt/PZT$ 30/70 1 hour

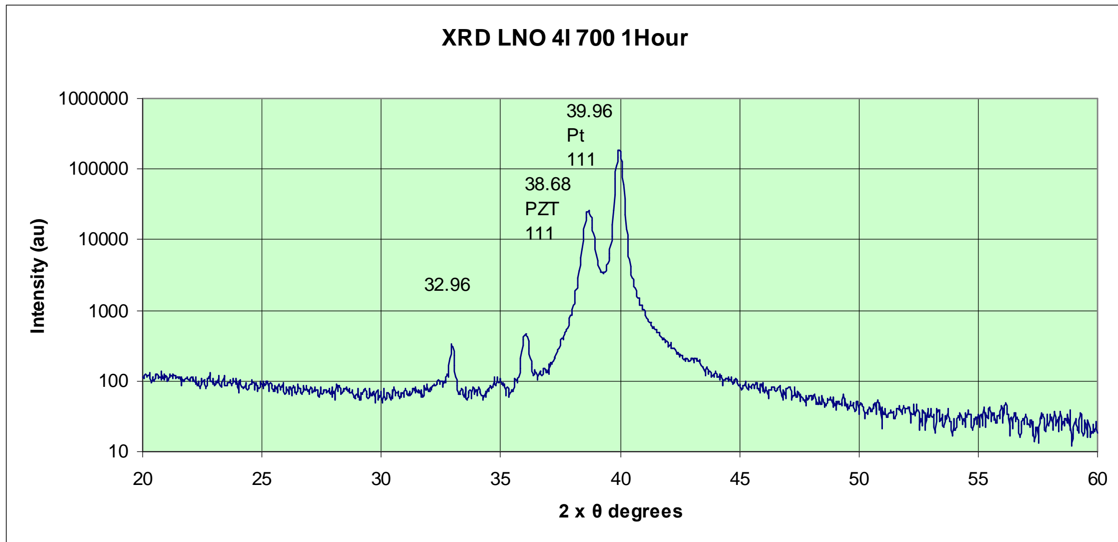

4.2.2.4 LNO Trial Four

Trial 4 was conducted with three layers of LNO deposited on top of 50nm of platinum, which itself was on PZT 30/70. This was to examine the possible inclusion of LNO as a potential barrier layer in consort with platinum. Pyrolisation was conducted for two minutes at a temperature of 350°C. Crystallisation was conducted for five hours and 2 minutes at a temperature of 550°C.

Figure 4-8 LNO Trial 4 XRD LNO on Pt/PZT 70/30

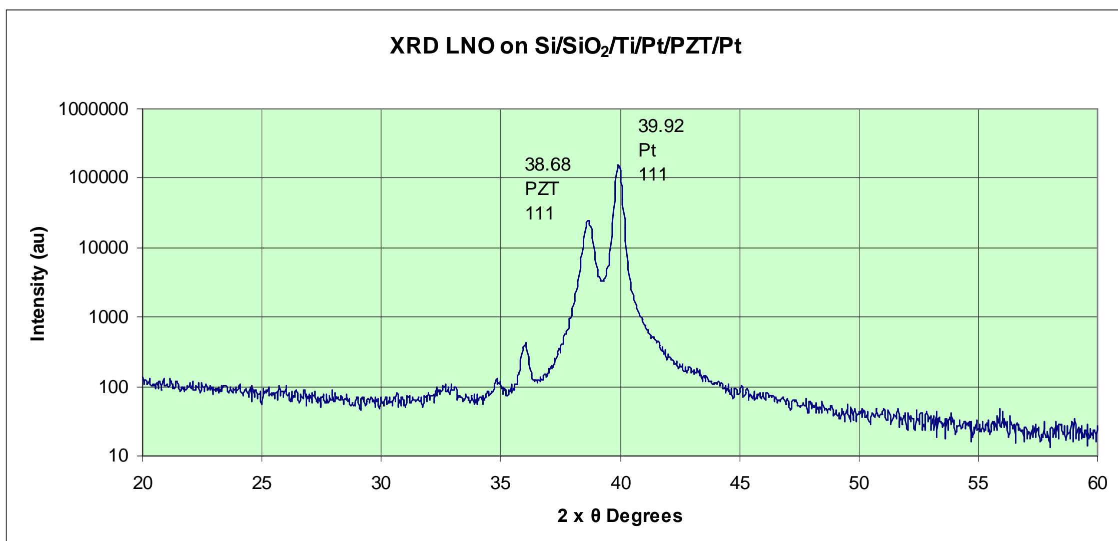

Again, the XRD shown above as Figure 4-8 does not show any crystallographic evidence of LNO presence.

4.2.2.5 LNO Trial Five

The principle element of this trial were the elements of a more stringent cleaning strategy and the use of rapid thermal annealing to see if the effects of radiant crystallisation would yield results.

The cleaning regime consisted of substrate degreasing and refluxing with ultra-pure isopropanyl (IPA). The procedure started in the laboratory with the samples being washed with detergent and water, followed by washing with copious amounts of distilled water. Thereafter, the samples were subject to ultrasonic cleaning for three minutes; firstly in distilled water; then in acetone and lastly, another three minutes in IPA. When this stage was complete the samples were transferred to the clean room where refluxing would take place.

The refluxing method requires a receptacle for heating ultra pure IPA and a condenser column so that the samples are subject to cleaning with distilled IPA. This process was repeated twice and the samples were left overnight so that the apparatus could cool down.

This trial used two samples cleaned in the meticulous fashion outlined above. The experimentation was conducted with three layers of LNO deposited on top of PZT 30/70 with pyrolisation for five minutes at a temperature of 350°C. Crystallisation was conducted by Rapid Thermal Annealing (RTA) for 3 minutes at temperatures of 500 and 600°C.

Figure 4-9 LNO Trial 5 XRD LNO PZT 30/70 RTA 500°C

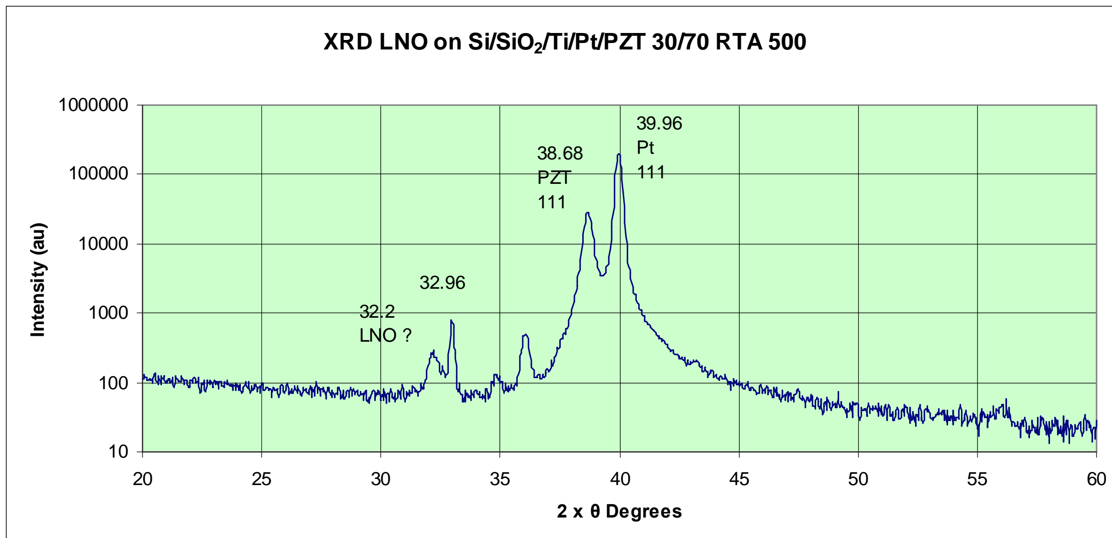

Interestingly, there is a difference in XRD's for these samples, which were identical in all respects except the crystallisation temperature. The XRD shown above as Figure 4-9 indicates a presence around the value of 32/33° for 2θ for the sample subjected to 500°C crystallisation that is not there for the sample subjected to 600°C crystallisation, which is shown below as Figure 4-10.

Figure 4-10 LNO Trial 5 XRD LNO PZT 30/70 RTA 600°C

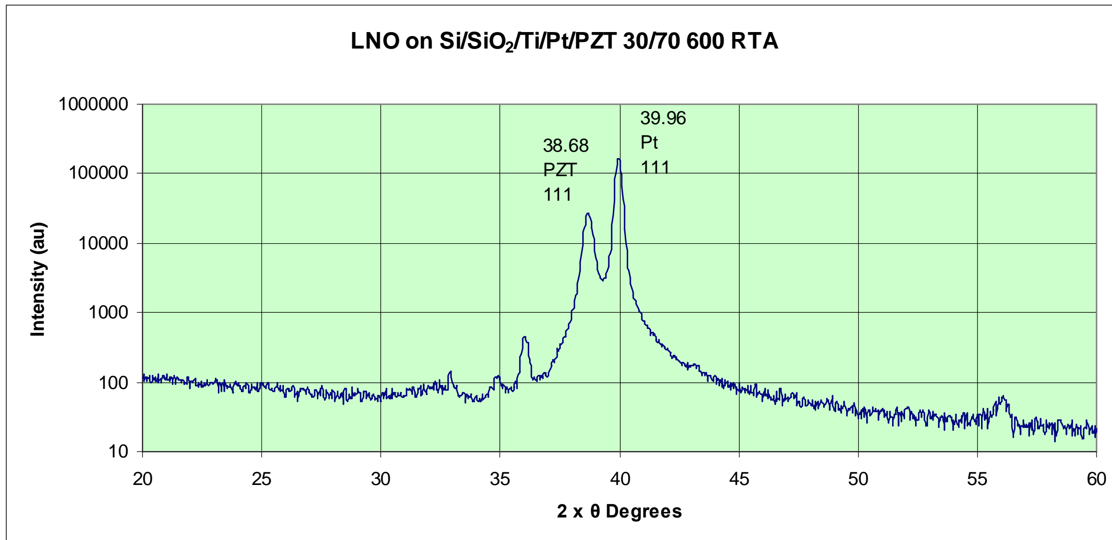

A representative sample of the surface of the specimens subjected to LNO deposition is shown below as Figure 4-11 with images taken by an optical microscope. The images show the general cracked and blistered demeanour of the surface, which is also peeling.

Figure 4-11 Representative Sample of LNO surface conditions.

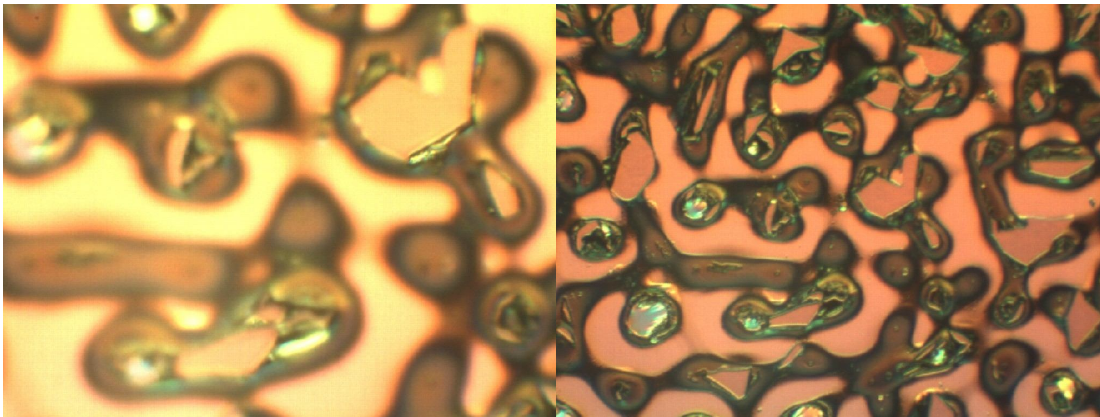

4.2.2.6 Summary of LNO trials

As the experiments investigated the effect of various crystallisation temperatures, conditions and methods of application, with no tangible results, it is difficult to state anything remotely promising for the deposition of LNO by CSD for the top electrode on top of PZT. All of the structures were crack ridden and there were no real suggestions of LNO presence with XRD analysis. However, LNO has never been deposited by CSD as a top electrode on top of PZT. So, perhaps it is no surprise. In mitigation, the sol is old, as it was synthesised in 2005 it may not be active now.

The one positive aspect is through the indication that LNO may be present in an amorphous form. Perhaps this gives some scope for further investigation particularly in light of the findings in trial five with crystallisation by RTA. In this case the samples were identical in all aspects except the crystallisation temperature, and there is a difference in the XRD analysis of the samples. This particular trial also highlights that successful results may be achievable with the advent of a more intense cleaning regime.

4.3 Ruthenium Oxide

A ruthenium target was available courtesy of the coatings group within the department. However, borrowing the use of a target and using one of the group's sputtering machines meant that only one run at deposition was possible. Hence, with the benefit of experience from some LNO deposition previously it seemed sensible to deposit onto glass slides so that some XRD analysis could be made on ruthenium oxide alone (without the strong presence of platinum and PZT). Lim et al. (Lim et al., 1999) report XRD peaks at values around 28° and 54° for (110) and (211) orientations, respectively.

The cleaning regime for the RuO_2 deposition was the stringent one outlined above which includes substrate degreasing and refluxing with ultra-pure isopropanyl (IPA). This was conducted on two glass slides and samples of both variants of PZT, 52/48 and 30/70.

4.3.1 RuO_2 Deposition

The ruthenium oxide electrode was deposited with a 5cm 99.995% pure ruthenium target and pulsed DC Magnetron sputtering using a Leybold L560 vacuum system with a base pressure of 5.7×10^{-7} Torr. The sputtering conditions were 180W using a 1.6 μSecond pulse width at a frequency of 200 KHz. The DC was pulsed to avoid oxidation of the target. The gas supply was an 80/20 Ar/O_2 mixture with a flow rate of 241 SCCM under a sputtering pressure of 5.1mTorr. The Ruthenium deposition was conducted by Jeff Rao.

The samples were subject to 10 Minutes pre-cleaning. The variations in voltage and current over the deposition cycle are given in the table below.

Table 4-1 Ruthenium Oxide processing

Time	Voltage/V	Current/A
15:15	407	0.44
15:18	423	0.43
15:25	427	0.42
16:25	424	0.41

4.3.2 RuO_2 Analysis

Once the deposition process was complete RuO_2 analysis could begin. The first aspect to discover was the thickness of RuO_2 deposited this was achieved with the Taylor Hobson Tallysurf system which gave a thickness of 1.6μm.

4.3.2.1 Analysis of RuO_2 deposited on Glass slides

The next stage was to characterise the samples with XRD analysis, which is shown below as Figure 4-12. Thereafter, the samples were subjected to annealing, initially with the glass samples to see the effect of different temperatures.

Figure 4-12 XRD of RuO_2 on glass slide

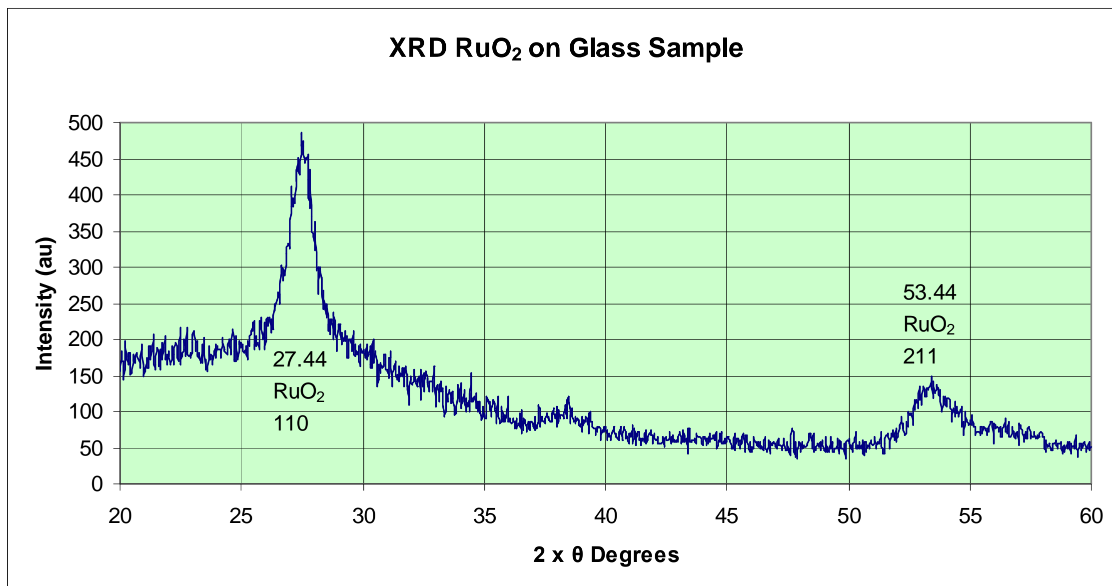

Analysing the RuO_2 on glass gives the opportunity of identifying where the peaks are likely to occur without the impact other elements being present. Once characterised the glass samples were subjected to differing temperatures of annealing to see the effects of temperature on crystallisation. All annealing was conducted for thirty minutes using the Sawntec HP-160/700 system.

The XRD analysis of sample 1, of RuO_2 on a glass slide, subject to annealing at a temperature of 450°C is shown below as Figure 4-13.

Figure 4-13 Sample 1 RuO_2 on Glass Slide annealed at 450°C

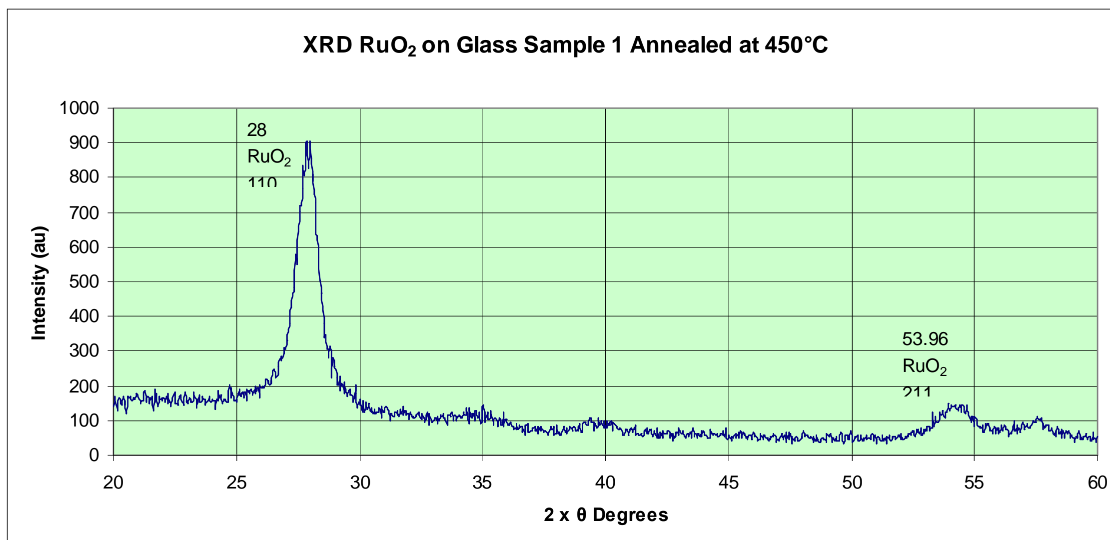

The XRD shows that annealing at 450°C, for thirty minutes, gave a more intense peak and gives values for 2θ that are more in tune with the values expected from literature, for crystallised RuO_2.

The second sample for RuO_2, on a glass slide, was subjected to annealing at a temperature of 550°C and the XRD analysis for this is shown below as Figure 4-14.

Figure 4-14 Sample 2 RuO_2 on Glass Slide annealed at 550°C.

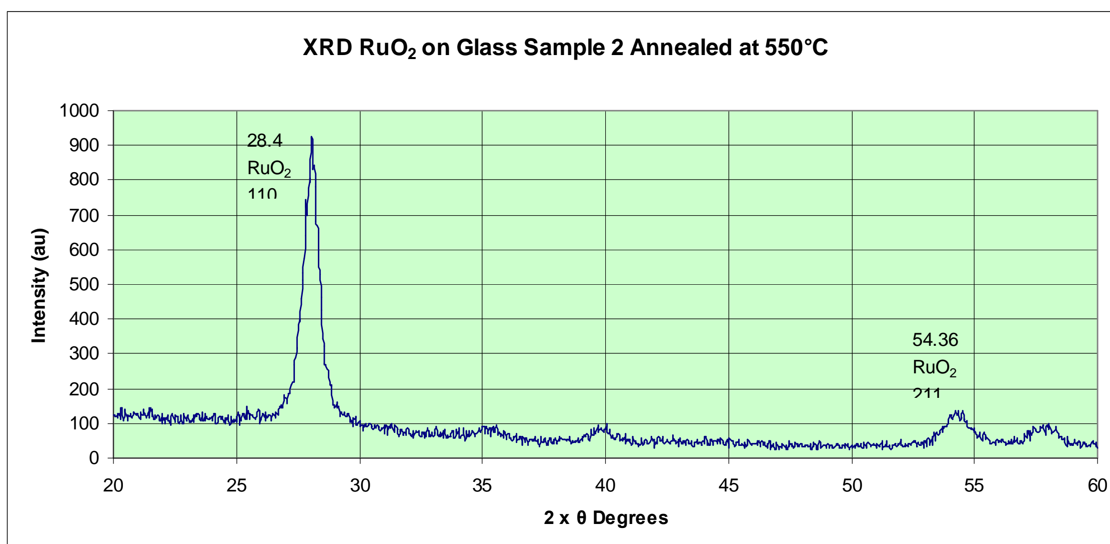

The peaks are more intense after annealing at the higher temperature. The values for 2θ are slightly different which could be explained by the glass being bowed by the effects of compressive strain brought on by annealing. Sample 2 was larger than sample 1 so the effect was amplified.

4.3.2.2 Analysis of RuO_2 deposited on PZT 30/70

Armed with knowledge obtained from analysis of the RuO_2 samples prepared on glass slides, the attention now turns to the depositions on PZT.

XRD was conducted on the RuO_2 deposited on PZT 30/70 sample both prior, and subsequent to annealing.

The XRD analysis of RuO_2 deposited on PZT 30/70 prior to annealing is shown below as Figure 4-15, in linear form. It gives an indication of the problems associated with analysing materials with a weak intensity against strong intensity materials like PZT and platinum.

Figure 4-15 XRD Analysis (Linear version) of RuO_2 deposited on PZT 30/70

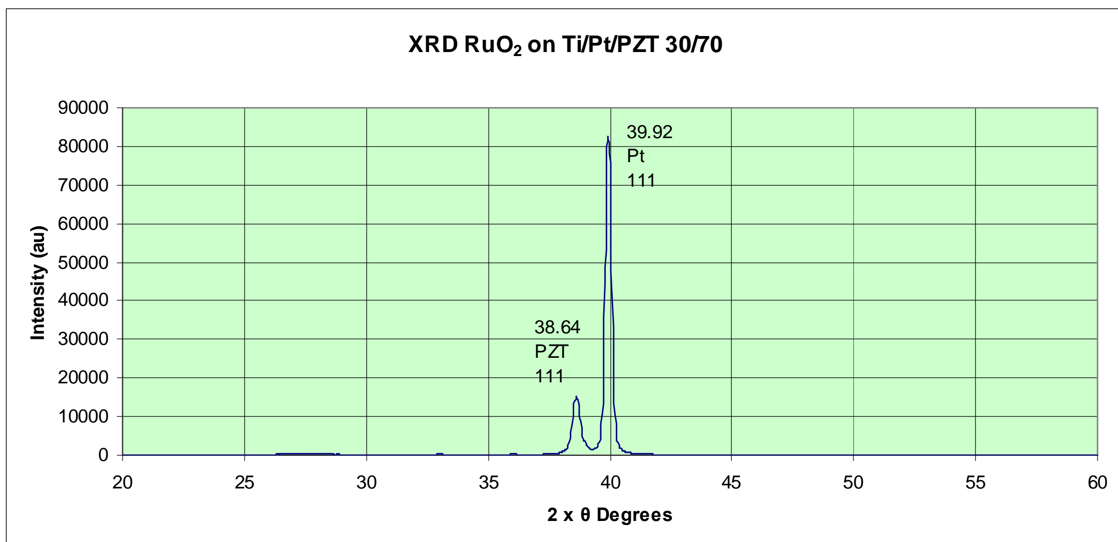

It is only with XRD analysis in logarithmic form that RuO_2 is clearly evident, as shown in Figure 4-16 below.

Figure 4-16 XRD Analysis (Logarithmic version) of RuO_2 deposited on PZT 30/70

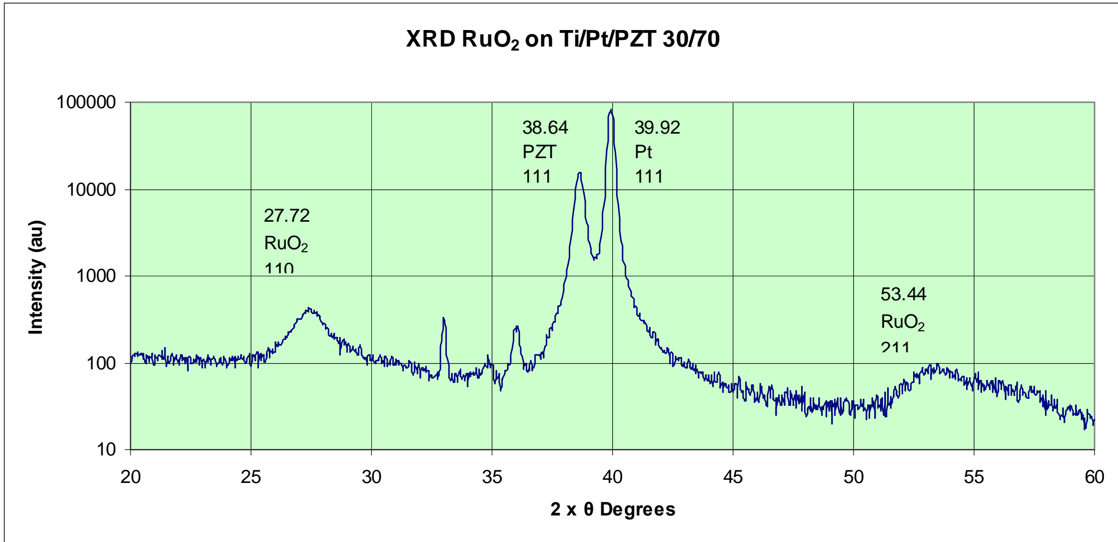

The samples of RuO_2 on PZT 30/70 were then subject to the same annealing conditions as those for the glass samples. The XRD analysis conducted on the sample after annealing is shown below as Figure 4-17.

Figure 4-17 XRD Analysis (Linear version) of RuO_2 deposited on PZT 30/70 after annealing at 450°C for thirty minutes.

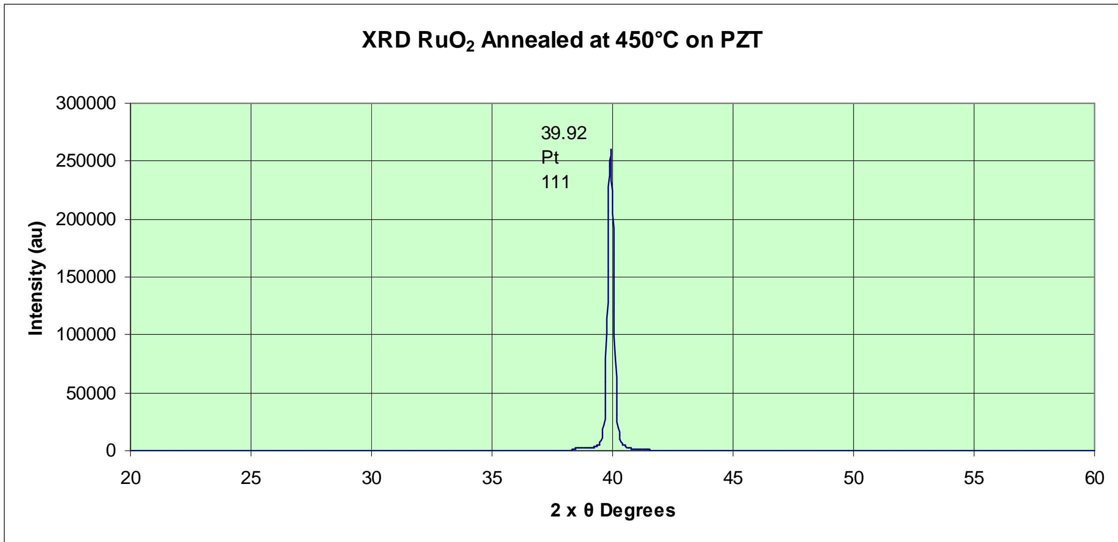

The linear analysis shows that the PZT is absent after annealing at 450°C. The logarithmic version below gives more of an insight in that there is a presence but it has been stripped off in places by the stresses caused by the annealing process.

Figure 4-18 XRD Analysis (Logarithmic version) of RuO_2 deposited on PZT 30/70 after annealing at 450°C

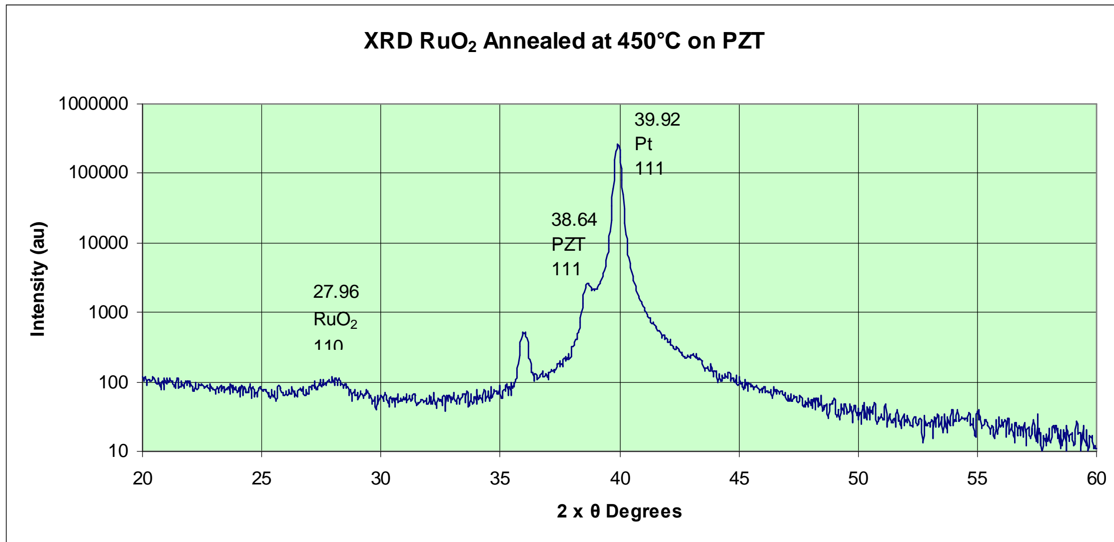

This sample was analysed using optical microscopy and an image was taken of the surface which is shown below. There are three distinct materials observable, with areas of platinum, ruthenium oxide and PZT. The stress from the thickness of ruthenium oxide deposited, allied with being annealed at 450°C for thirty minutes has overwhelmed the underlying PZT to reveal platinum.

Figure 4-19 Image of surface of RuO_2 deposited on PZT 30/70 after annealing at 450°C

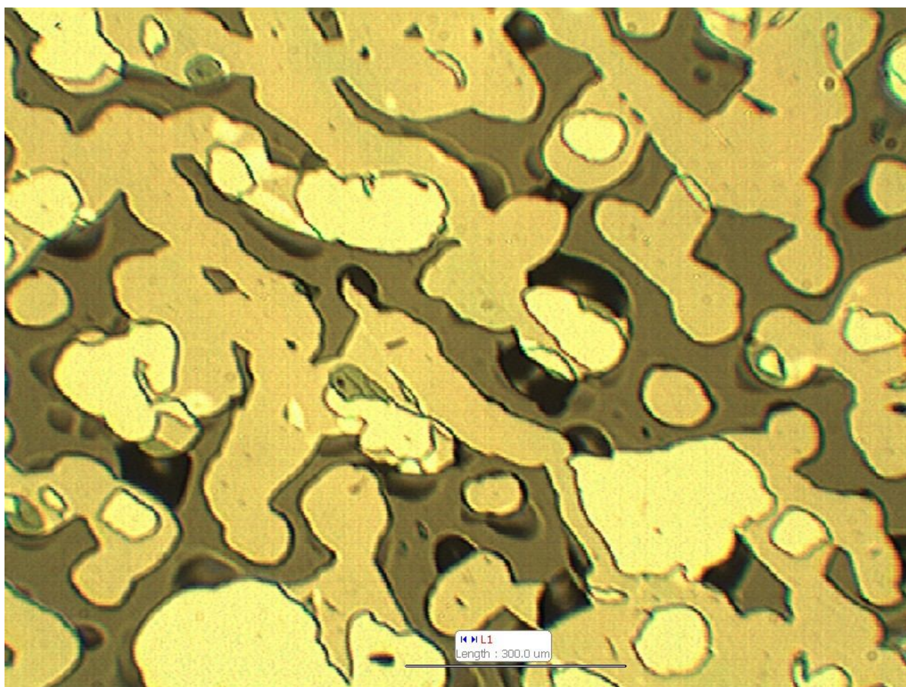

Following this, analysis was conducted on the other sample of RuO_2 deposited on PZT 30/70 after annealing at 550°C. The XRD analysis in logarithmic form is shown below.

It shows that this sample faired better after the annealing process as there is still clear evidence of PZT and there is a more intense aspect to the RuO_2.

Figure 4-20 XRD Analysis (Logarithmic version) of RuO_2 deposited on PZT 30/70 after annealing at 550°C

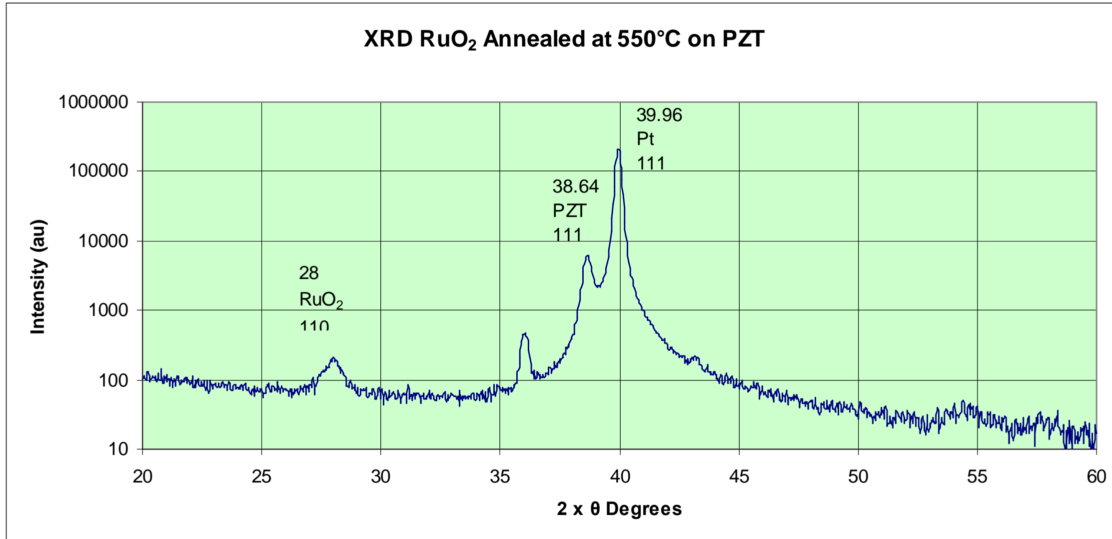

4.3.2.3 Resistivity Measurements for Ruthenium Oxide

The resistivity of the ruthenium was calculated using measurements taken with the four point probe. Measurements were made for the two samples of ruthenium oxide on glass slides both before, and after annealing. In this way it was possible to investigate the effect of annealing temperature on resistivity.

The four point probe method is based on the work of Valdes with his work on resistivity measurements in respect to germanium.(Valdes, 1954).The principle uses four equally spaced tungsten probes to make contact in a line on the surface under test. Thereafter, a floating potential is measured over the inner two probes as a result of applying a current to the outer pair of electrodes. The measurement yields a sheet resistance value and when multiplied by the thickness of the material a value is obtained for the resistivity (Ωcm) of the material under test.

The measurements were taken over a range of currents to ascertain whether there was a linear dependency for voltage/current characteristics. The recorded values are included in appendix B as are graphs of the V/I characteristics. Reference, measurements from the four point probe were also taken for a sample with chrome/gold as a top layer.

Based on the sheet resistance in Ωcm calculated for the voltage measured at 0.5mA the resistivity was calculated by multiplying by the thickness of the RuO_2 layer (1.6μm). The resistivity of the respective samples was;

- Gold Reference = 3.6μΩcm
- RuO_2 Sample1 before annealing = 116 μΩcm
- RuO_2 Sample1 after annealing at 450°C = 74.56μΩcm
- RuO_2 Sample2 before annealing = 105μΩcm
- RuO_2 Sample2 after annealing at 550°C = 38μΩcm

These figures show that resistivity improves on annealing. The values themselves are excellent and are of the right order in comparison with values available from literature. Indeed, Izyumskaya et al.(Izyumskaya et al., 2007) quote a potential figure of 12μΩcm for ruthenium oxide. However, the values may have been skewed by the accuracy of the thickness measurement.

4.3.2.4 Summary of Ruthenium Oxide activity

The results of the investigation of ruthenium oxide were that conductive ruthenium oxide can be deposited from a ruthenium source in a mixed argon/oxygen atmosphere. The effects of annealing were also investigated at temperatures at 450°C and 550°C with XRD analysis. This gives evidence that the annealing gave larger grain sizes and a more intense peak indicates better crystallisation.

Resistivity measurements made with the four point probe on the glass samples indicate that the ruthenium oxide is conductive and the effects of annealing are to improve the conductivity. The resistivity figures changed from 116μΩcm to 74.56μΩcm for the sample annealed at 450°C, and changed from 105μΩcm to 38μΩcm for the sample subject to annealing at 550°C.

As the deposition thickness was so large, the added thermal stress from annealing was sufficient to tear the underlying PZT from the samples. The XRD shows the presence of all three components and an image taken with the optical microscope reveals three distinct areas on the sample surface.

Unfortunately, the effect of stress induced delamination in areas of the sample prohibited any further investigation in ruthenium oxide as a top electrode on PZT.

4.4 Adhesion Methods

The methods for adhesion analysis were limited. These options consisted of scratch testing using a nanoindenter and a wide area pull test using a PAT Model GMO1 Adhesion tester.

4.4.1 Pull Test

All pull tests were conducted with a PAT Model GMO1 Adhesion tester. The pull tester uses studs to affix to the sample under test. The studs available were 14.1mm and 20mm which are calibrated to give 40MPa full range deflection and 20MPa full range deflection, respectively.

4.4.1.1 Sample Preparation

The sample preparation method for the pull test is time consuming and laborious. The method evolved over a period of weeks after repeated attempts and failures. The requirements for the presentation of the test specimen to the test system are that the sample has to be affixed to a base so that the test head has enough area to pull on and in addition the stud has to be affixed to the sample so that the pull test can measure the adhesion at the weakest point of failure. The picture below, presented as Figure 4-21, shows a completed test specimen ready for test.

Figure 4-21 Test specimen ready for pull test

The adhesives used were of the two part epoxy type. Two variants were tried with differing set times, in order to attempt to speed up the process. However, it was found over a number of trials that the quick setting epoxy did not possess enough bond strength to perform the test, as the weakest point of adhesion was in the epoxy/stud interface. One method to improve the adhesive's bond strength and quicken the set time was by using a hot cupboard permanently in the 40°C-plus region of temperature.

When the process failed it meant another tiresome and time consuming process to remove the epoxy from the test stud and sample surface. Dichloromethane was used as a solvent for the epoxy based adhesives. However, swabbing the epoxy off of the surfaces was still a time consuming task.

As the procedure evolved it became evident that the sample had to be affixed to the base whilst the epoxy was fresh so that the underside of the sample was guaranteed to have complete coverage of the epoxy in its connection with the base. In addition, this had to

be complete with the sample affixed, and the epoxy fully set, before affixing the test stud.

The test stud/sample interface required the epoxy to have thickened and set a little otherwise the relatively heavy test stud would slide off of the surface of the sample. This is caused by the sample surface being smooth and shiny, and the fresh epoxy acting as a slight lubricant for the comparatively heavy stud.

4.4.1.2 Pull Test Results

The samples presented to the pull test and the values obtained are shown below as Table 4-2.

Table 4-2 Pull Test results

Sample	Value
Si/SiO_2/Ti/Pt	No values obtained
Si/SiO_2/Ti/Pt/PZT with etch-back	5MPa and 6MPa
Si/SiO_2/Pt	2MPa
Ti/Pt PZT 30/70/Pt	3MPa

In all of the tests conducted on titanium/platinum samples the adhesive failed at the stud interface before the layer delaminated. However, of the samples tested some of the adhesive failures were greater than 6MPa which had no relevance until some results were obtained for the titanium/platinum PZT sample with etch-back. Two of these produced measurable values, with the highest value being 6MPa.

The Si/SiO_2/Pt sample was a random sample that was spare and it provided an early test to see if the method could produce a result. The last specimen to produce a value was a platinum top electrode sample which recorded a value of 3MPa.

4.4.1.3 Summary of pull test method

Although the sample group is small and the test produced few tangible results, some comparative judgements can still be drawn.

In analysing the pull test, some of the results obtained concern the events of failure as well as those of success. The tests on titanium/platinum that had stud/sample adhesive failure had higher values in failure than the results recorded for the titanium/platinum ensembles with PZT and etch-back. So, there is some comparable analysis of the impact on adhesion from the extrinsic stresses caused by CSD deposition.

A direct comparison is possible with platinum and titanium/platinum based electrodes because the titanium/platinum electrode with PZT and etch-back, produced higher measured values than either of the platinum samples. Thus, confirming the benefits, and need, of the titanium adhesion layer.

The pull test produced some measurable results but it is not an entirely satisfactory method for measuring the adhesion of thin films because of the inherent problems associated with shiny films and adhesive contact.

Considering the time taken to prepare the sample for test and the time spent cleaning the samples when adhesive failure occurs, one of the judgments drawn on the method has to be that; whilst not wholly unsatisfactory in determining the failure of thin metal films it is an expensive process in terms of time.

4.4.2 Scratch test

The sample sent for scratch testing had patterned annealed platinum as a top electrode. The objective of this was twofold as the results would determine whether the scratch test is a viable option for testing electrodes on PZT and whether it is possible to determine the impact of patterning on electrode adhesion. Otherwise, there are no other options available to test small area patterning as the pull test works over a wider area than the patterned electrodes.

The multiple pass wear scratch test was the test option available as the critical load module is not available on the Nanotest 600 indenter at Cranfield. A diamond stylus with a 250nm spherical tip was used to conduct the experiment. The pre-test involves levelling the scan against a light load ramped to 400mn at 5mn/second. The result for the multiple wear scratch test conducted on the patterned platinum electrode is shown below as Figure 4-22.

Figure 4-22 Multiple pass wear scratch test on Platinum contacts

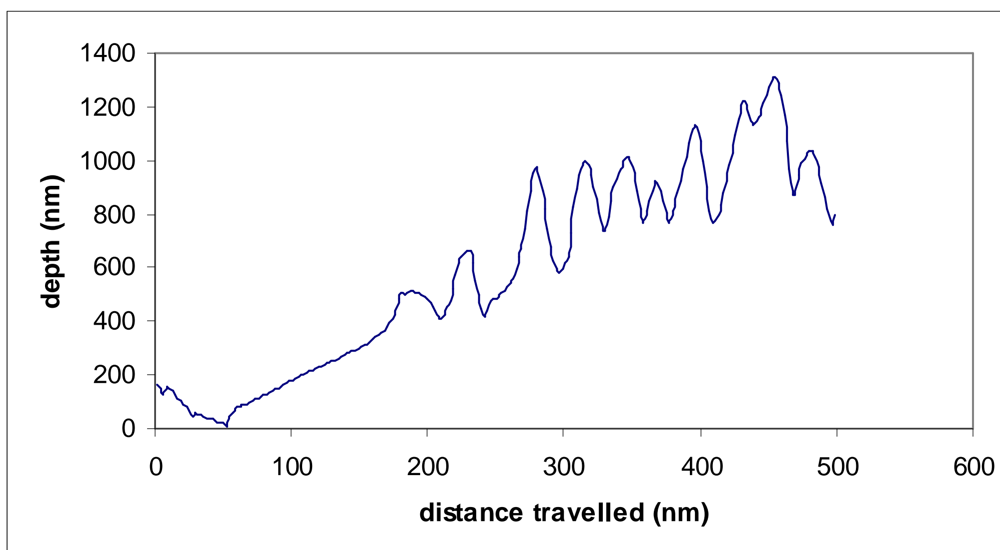

The results show an immediate deformation under load and then some recovery. What is clearly evident is that the patterned electrode has failed immediately that the load has

been applied. The recovery is evident that it is already through to the underlying PZT layer.

The wear test is generally used to simulate the impact of wear in service to give some indication of product performance. This clearly shows that there is a problem with the patterned platinum electrode and would indicate that in-service this would only get worse.

In judging the method it is unclear whether the test is unviable in testing 100nm electrodes, or whether it is as a result of testing an electrode on PZT. In either case the main conclusion is that the scratch testing options available at Cranfield are not useful for determining results in relation to thin (100nm) films, certainly on PZT.

Unfortunately, as there was a breakdown on the scratch tester no further analysis was possible. It would have been useful to test the samples of titanium/platinum and titanium/platinum with etch-back to see if the test was viable with thin films on a silicon based substrate rather than on PZT and whether it would show any comparative values between the samples.

4.5 Stressed Overlayer

In order to investigate the effects of using a stressed overlayer various samples were cleaved into strips. The samples chosen for this study were Si/SiO_2/Ti/Pt, Si/SiO_2/Ti/Pt/PZT 30/70 with the PZT removed (with HF), Si/SiO_2/Ti/Pt/PZT 30/70/Pt and Si/SiO_2/Ti/Pt/PZT 30/70 Cr/Au.

In order to produce delamination in the form of telephone chords or blisters we require a material which sputters with compressive stress. Originally, this was conceived with Chromium in mind as this is well known for producing large values for stress and is used extensively in the literature reviewed previously. However, the prevailing consensus is that sputtering chromium using the Nordiko machine produces chromium with a tensile stress.

As the samples had already been mounted and pressured down the decision was made to use another target material. For this reason the stressed overlayer material used for this experiment was platinum. An added advantage being that the material is well characterised for this machine as it is used extensively as an electrode material. Also, it sputters quickly so the run time on the machine is minimised.

4.5.1 Stressed Overlayer Sputtering parameters

In order to make sure that the platinum superlayer adhered to the samples under test, a 10 nm chromium adhesion layer was deposited using a size 8” x 4” rectangular 99.999% pure chromium target. The chromium was deposited with RF sputtering using a Nordiko 2500 System with a base pressure of 5.7 x 10^{-7} Torr. The pre-sputter

conditions were 300W with a D.C. bias of 1.8V and 200W for the last minute with a D.C. bias of 1.4V. Argon gas was used for the plasma with a flow rate of 40.9 SCCM under a sputtering pressure of 10mTorr. For a deposition of 10nm the target was exposed for 30 Seconds.

Without breaking vacuum the platinum deposition took place with a 99.999%, 8” x 4” platinum target using DC magnetron sputtering at a voltage of 445V and a current of 0.7A. The deposition rate for platinum is 1.13nm per second. So, to deposit platinum coatings of 250nm, 500nm and 750 nm we required 3 minutes 41 seconds, 7 minutes 22 seconds and 11 minutes 3 seconds, respectively. These timings were calculated using the rate above. Unfortunately, under further scrutiny this is the rate for 0.4A and the actual rate for 0.7A is 2.05nm per second. So, the amended figures are 453nm, 906nm and 1.359μm.

4.5.2 Stress Measurements for stressed overlayer

The values of delta (the beam’s deviation from horizontal) were taken using a Dektak surface profiler for 15mm length of scan. All measurements were recorded for each sample because the application of a stressed layer may have affected any of the samples.

Table 4-3 δ values of samples before the Stressed Overlayer test

$Si/SiO_2/Ti/Pt$ δ (Angstrom, Å)	Ti/Pt/PZT 30/70 with Etch-back δ (Angstrom, Å)	Ti/Pt/PZT 30/70 /Pt δ (Angstrom, Å)	Ti/Pt/PZT 30/70 /Cr/Au δ (Angstrom, Å)
4892	-2174	4101	-6804
5342	-2132	4614	-5600
5040	-2974	4720	-6353

Measurements for δ give an indication of the effects of deposition and processing on the various electrode structures with positive values indicating compressive stress and negative values indicates tensile stress. Thus, the titanium/platinum deposition by sputtering is compressive, in concurrence with that shown in the previous chapter with the full wafer. Also, the effects of CSD processing on the titanium/platinum bottom electrode serve to make it tensile. Additionally, the sputtered platinum top electrode is in compressive stress and the effects of thermal evaporation for the deposition of the chrome/gold electrode serve to make it tensile.

To calculate the stresses induced by the overlayer measurements further values were taken for curvature delta using a Dektak surface profiler for a 15mm length of scan on the $Si/SiO_2/Ti/Pt$ without PZT deposition. These became the reference values for the stress calculations before and after stressed overlayer application.

This gave delta (δ) values of 20882Å, 22630Å and 25528Å for the stressed overlayer thicknesses of 453nm, 906nm and 1359nm, respectively.

The stresses were calculated using a one dimensional beam model derivation of the Stoney formula. So for stress in the film σ_f, the Stoney formula simplifies to the following;

Equation 4-2 Stoney One Dimensional Beam Model

$$\sigma_f = \frac{E_s t_s^2}{6Rt_f}$$

Where R is The Radius of curvature, and for the one dimensional model $R = l^2 / 8\,\delta$; E_s is the elastic modulus in the stretch direction for a (100) wafer which is $E_s[110]$ = 169GPa; t_f and t_s are the film and substrate thicknesses, respectively.

Table 4-4 Values for stress related parameters in Stressed Overlayer (SO) application

$Si/SiO_2/Ti/Pt$ δ/ (Å)	Radius of curvature before SO /m	Radius of curvature after SO /m	Stressed Overlayer Film Thickness/ nm	Stress before overlayer $Si/SiO_2/Ti/Pt$ /Mpa	Stress after overlayer $Si/SiO_2/Ti/Pt$ /MPa
4892	57.49m	13.47m	453	726.6	9.85
5342	52.65m	12.43m	906	793.5	5.81
5040	55.8m	11.03m	1359	748.5	4.33

4.5.3 Qualitative Results of Stressed Overlayer

The Ti/Pt bottom electrode pairing and the Cr/Au top electrode pairing were unaffected by the application of a stressed overlayer of Platinum. The Platinum top electrode on top of PZT, was unaffected by the stressed overlayer in that it did not blister in any way but was weakened to such an extent that it peeled when the tape affixing the samples

was removed. This occurred for all of the samples irrespective of stressed overlayer thickness.

Figure 4-23 below shows an image taken with an optical microscope showing the edge of the platinum top layer peeling away from the substrate when the tape was removed, which produced the only tape test failures in the project.

Figure 4-23 Platinum peeling after stressed overlayer

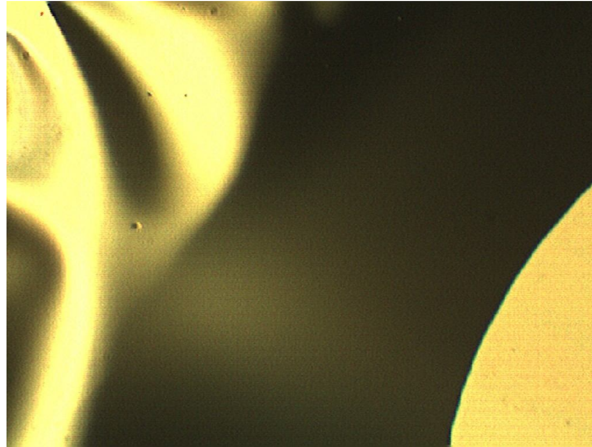

The Ti/Pt samples with PZT 30/70 deposition and etch-back were affected by the 906nm and 1359nm stressed overlayer depositions. The effects were in the form of various types of blister formation.

The various blister formations resulting from a stressed overlayer thickness of 906nm are recorded below in Figure 4-24 with images taken by an optical microscope.

Figure 4-24 Blister formation from 906nm Stressed Overlayer deposition on /Ti/Pt/PZT 30/70 with Etch-back.

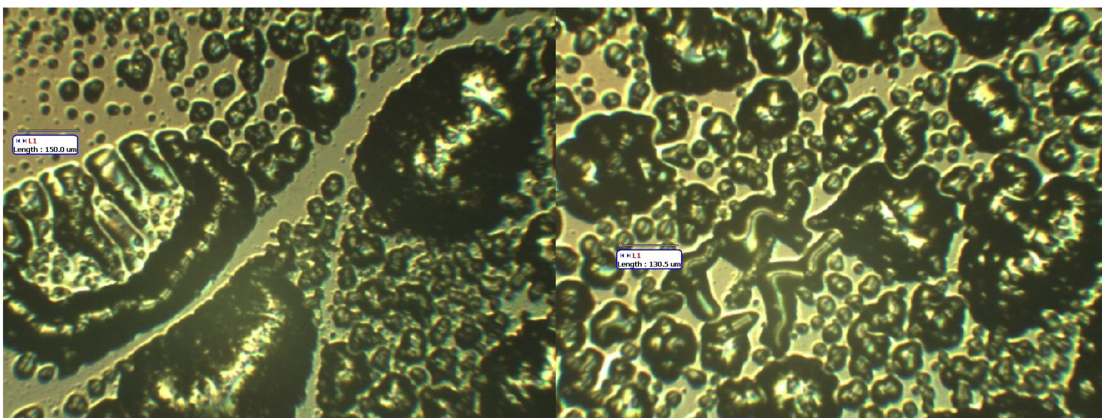

Also, on the samples that were subjected to 906nm of stressed overlayer deposition were what appeared to be some telephone chord-like blistering. Telephone chord type

blistering is generally considered to form because it is energetically favourable. This is shown below as Figure 4-25.

Figure 4-25 Processed Ti/Pt with blisters and telephone chord-like Formation

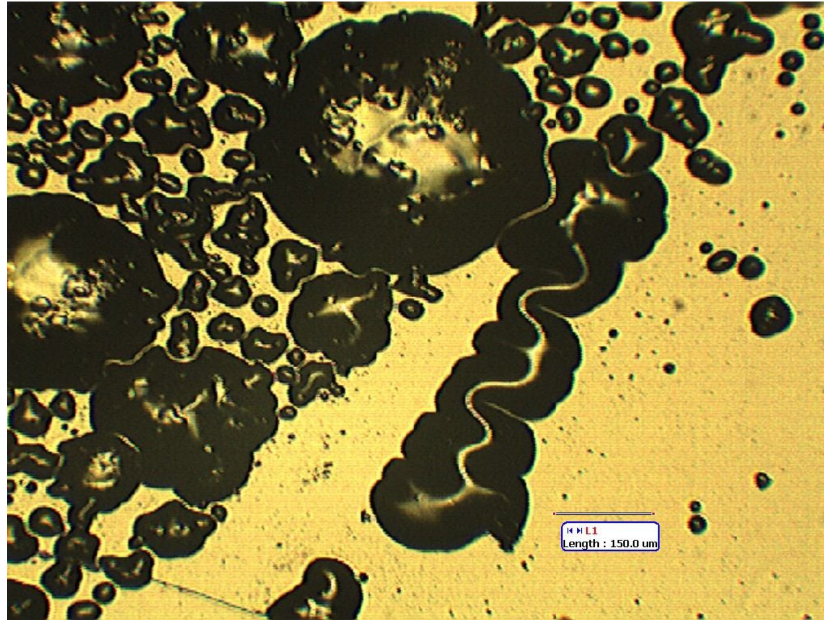

4.5.4 Blister Analysis

Using the microscope an isolated blister was found that looked almost perfectly circular, subsequently this blister was located on the Dektak surface profiler. The images of this blister taken with the optical microscope and Dektak surface profiler are left and right, respectively in Figure 4-26 shown below.

Figure 4-26 Image of circular blister with microscope and Dektak

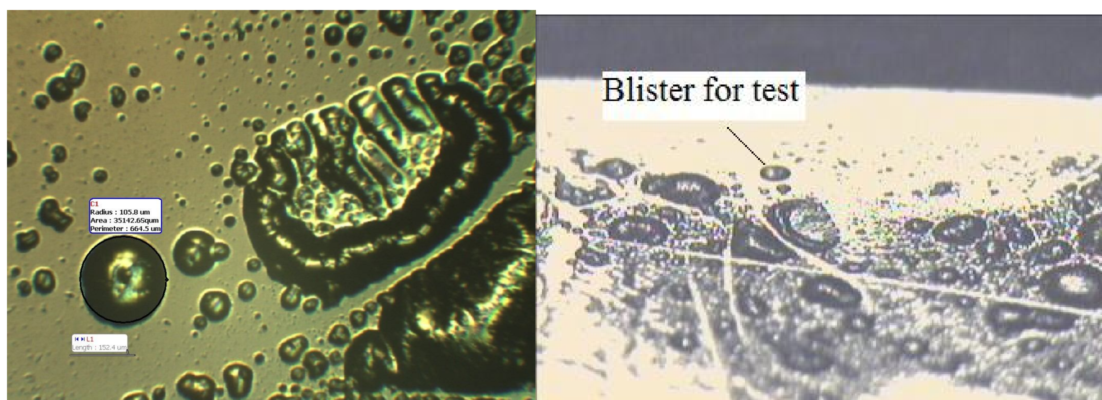

Having isolated the blister, the Dekatk surface profiler was used to measure the height and diameter of the blister using a 500µm length of scan. The scan profile produced is shown below as Figure 4-27 and the results gave a diameter of 240µm with a blister

height of 9000 Å. The stylus force was 30mN and the initial findings from this are that the blister did not break with this force.

Figure 4-27 Scan profile of Blister from Dektak

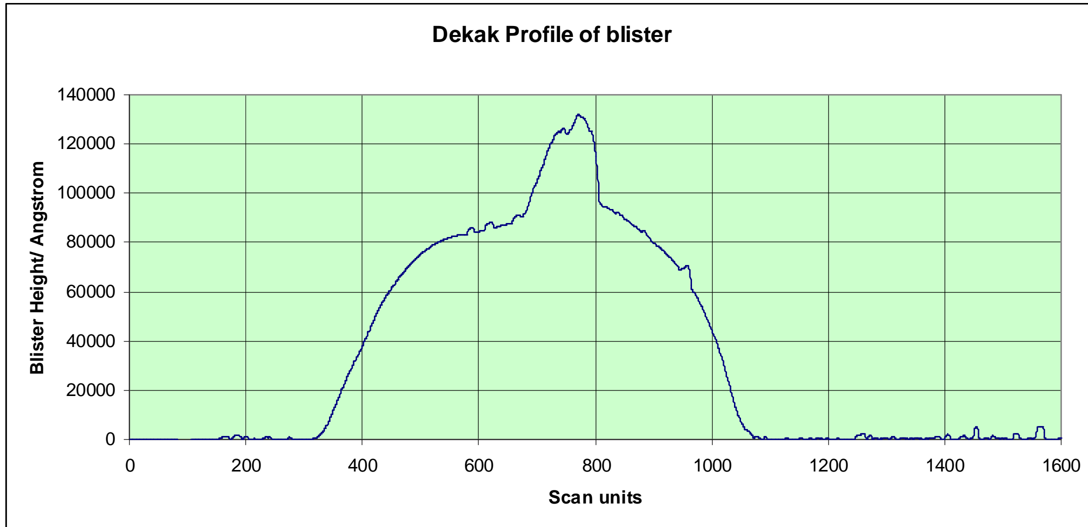

4.5.5 Work of Fracture

Using Cordill et al. (Cordill et al., 2007) the blister is akin to the deformation used in their model for a straight-straight buckle of uniform width and height with measurements taken through the centre.

So, for the measurements taken on the circular blister the values for the critical buckling stress σ_b and the residual stress of the buckle film σ_r are given by the following

Equation 4-3 Critical buckling stress σ_b

$$\sigma_b = \frac{\mu^2 E}{12(1-\nu^2)} \left(\frac{h}{b}\right)^2$$

And

Equation 4-4 Residual stress of the buckle film σ_r

$$\sigma_r = \sigma_b \left[c_1 \left(\frac{\delta}{h} \right)^2 + 1 \right].$$

δ is the Buckle height = 9000Å; b is half buckle width = 120µm; υ is Poisson's ratio for platinum =0.38; E is the elastic modulus for platinum=168GPa; h is the film thickness = 906nm; and the constants $\mu^2 = \pi^2$ and c_1 = ¾;

Using these equations the critical buckling stress σ_b= 20.5MPa and residual stress of the buckle film σ_r = 35.67MPa

For this model and these results the interfacial fracture energy $\Gamma(\Psi)$ where (Ψ) is the mode mixity of normal to shear stresses, which in this case is given by;

Equation 4-5 Interfacial fracture energy $\Gamma(\Psi)$

$$\Gamma(\Psi) = \frac{(1 - \nu^2)h}{2E}(\sigma_r - \sigma_b)(\sigma_r + 3\sigma_b)$$

Where σ_b is the critical buckling stress = 20.5MPa; σ_r.is the residual stress of the buckle film = 35.67MPa; υ is Poisson's ratio for platinum =0.38; E is the elastic modulus for platinum=168GPa; h is the film thickness taken as 906nm

Giving an interfacial fracture energy $\Gamma(\Psi)$ = 4.358 x 10^{-3} J/m^2 for titanium/platinum when subjected to PZT and etch-back. However, the values for residual stress and buckling stress calculated using the blister measurements do not match the values calculated previously, using the beam model, in Table 4-4. So, the interfacial fracture energy calculated is unlikely to be valid on these grounds alone.

If we use the stresses calculated for titanium/platinum using the beam model and substitute the critical buckling stress σ_b as 5.81MPa and the residual stress of the buckle film σ_r as 793.5MPa.

This yields an interfacial fracture energy $\Gamma(\Psi)$ = 1.47 J/m^2 for 108nm of titanium/platinum when subjected to PZT and etch-back, which is a unique condition.

In order to make some comparison Moody et al.(Moody et al., 2007) quote a figure of 41 J/m^2 for their stressed overlayer test on SiO_2/Ti 17nm/Pt. However, the values of $\Gamma(\Psi)$ are dependent on the mixity of stresses (normal and shear), as well as the material

under test and its thickness so direct comparisons are viewed with caution. In addition, the value is calculated for a titanium/platinum electrode that has been subject to the extrinsic stresses caused by CSD processing so there are unlikely to be comparative figures.

There are caveats to the values calculated as they are based on the assumption that 906nm is the thickness for the onset of buckling which is not guaranteed. Ordinarily multiple tests would be made to target this value of thickness. However, there was no activity in the first sample subject to less deposition of platinum and the differences between the stress values are not so large. However, of course there is a significant difference in thickness.

4.5.6 Summary of Stressed Overlayer

In conducting the analysis associated with the stressed overlayer it has been shown that the titanium/platinum deposition by sputtering is compressive in concurrence with previous analysis. Also, the effects of CSD processing on the titanium/platinum bottom electrode serve to make it tensile. Additionally, the sputtered platinum top electrode is in compressive stress and the effects of thermal evaporation for the deposition of the chrome/gold electrode serve to make it tensile.

The application of a platinum stressed overlayer to the four sample types produced no blistering to any of the sample types for 453nm. However, there was blistering with the application of 906nm of platinum in the titanium/platinum electrode with PZT and etch-back but not with any of the other samples.

One quantitave assessment drawn from using the stressed overlayer is that the titanium/platinum electrode with PZT and etch-back is the only electrode with weak enough adhesion to be delaminated by the application of a stressed overlayer at thickness of 906nm with a stress of 5.81MPa and therefore the weakest of all the electrode structures presented for the test. A second, qualitative assessment can be drawn as the platinum top electrode was the only electrode type that suffered delamination with the extra force supplied when peeling the tape that affixed the samples to the stage for sputtering. So we can infer that this is the next weakest electrode structure of the samples presented for test. Therefore, we can also state that the chrome/gold electrode structure is preferable to platinum as a top electrode in terms of adhesion.

An attempt to calculate the work of fracture was conducted using analysis of an almost perfectly circular blister and applying the measurements to a model for a straight buckle of uniform width and height with measurements taken through the centre. In addition, the work of fracture was also calculated using the stresses generated from the Stoney derived one dimensional beam model.

5 Conclusions

This section forms the conclusions to the project and gives suggestions for further work. The individual elements that make up the work are concluded separately and they are followed by a brief summary of conclusions.

5.1 Conductive Oxides

The experimentation with LNO as a top electrode did not prove successful. As most variants for crystallisation were tried, CSD seems not to be suitable as a method of deposition on top of PZT. As this has never been accomplished anywhere, to the writer's knowledge, perhaps it is no surprise. In mitigation, the sol is old and was synthesised in 2005 so it may not still be active. In hindsight, it would have been sensible to conduct trials of the sol on top of silicon as this has been successful in the past. In the case of one particular problem, the layers showed evidence of cracking even after pyrolysis and the nature of cracking has been previously reported as a result of a lack of formamide.(Cheng et al., 2003)

The one positive aspect is through the indication that LNO may be present in an amorphous form. Perhaps this gives some scope for further investigation particularly in light of the findings when crystallisation was attempted by RTA. In this case the samples were identical in all aspects except for the crystallisation temperature, and there is a difference in the XRD analysis of the samples. The other feature of this investigation was the intensive cleaning regime associated with degreasing and refluxing. It is no coincidence that the ruthenium oxide was successfully deposited on samples that shared this cleaning process.

The conclusions that can be drawn from the investigation of ruthenium oxide were that conductive ruthenium oxide can be deposited on to PZT from a ruthenium source in a mixed argon/oxygen atmosphere. In addition, the investigations with the deposition on glass slides showed that annealing brought improvements in the figures measured for resistivity, as they changed from 116μΩcm to 74.56μΩcm for the sample annealed at 450°C, and changed from 105μΩcm to 38μΩcm for the sample subject to annealing at 550°C, a dramatic improvement. The resistivity values themselves compare well with the figures obtained from the literature.

Unfortunately, because of the thickness of the ruthenium oxide deposited on the PZT samples the added stress of annealing produced delamination in the underlying PZT, which prohibited any further analysis. However, the process is in place for further investigation and annealing temperatures have been investigated.

5.2 The in-situ bottom electrode

The XPS and depth profile analysis on titanium/platinum with PZT and etch-back reveals the presence of lead and there is some evidence of lead interdiffusion in the titanium/platinum electrode structure. This has real potential to impact on the adhesion of the electrode system to the PZT layer. It also has potential implications in performance of the electrode as part of the functional ferroelectric system. These facts lead to the suggestion that a more suitable barrier electrode is required. Perhaps there is a case for the introduction of conductive oxides for this reason alone.

The absence of any titanium in the XPS analysis allied with the information from the depth profile indicates that while some titanium diffusion is taking place there is no impact on the interface between the bottom electrode and the PZT. So, there is no hillock formation with 8nm of titanium and 100nm of platinum. However, the interdiffusion of titanium into platinum is another factor in the weakening of the titanium/platinum bottom electrode.

5.3 Adhesion Methods and their Results

The sample presented to the scratch tester was platinum with patterned electrodes on top of PZT. The immediate deformation of the electrode under the application of a small load, followed by the recovery gave clear evidence that it was already through to the underlying PZT layer. So, the method did not produce results of tangible value. What is unclear is whether the method is unviable in testing 100nm thin films, or whether it is a problem associated with an electrode structure on PZT. The machine’s breakdown meant that no further investigations were possible for thin films on silicon which would have been useful in assessing whether the method has merit.

One conclusion from the scratch test is possible however, in that the repetitive wear scratch test is generally used to indicate product performance in-service, and in those terms there is clear concern over the patterned platinum electrode.
Conclusions on the pull test method are that it requires laborious and time consuming preparation but it can produce some results of a qualitative nature. So it may have a place in a hierarchy of adhesion testing.

Conclusions on the results obtained from the pull test include some comparative values that were in the failure events in the test stud/sample interface as well as the recorded values from successful tests. The main conclusions drawn from these results include a confirmation that the PZT CSD process does have a deleterious impact on the adhesion of the titanium/platinum bottom electrode and the results for platinum show a definite need for an adhesion layer.

5.4 Stressed Overlayer

A consequence of conducting the analysis associated with the stressed overlayer technique has been to show the influence of deposition methods and processing on the various electrode structures examined by the technique.

The titanium/platinum bottom electrode deposition by sputtering is compressive and the effects of PZT deposition by CSD serve to make the electrode structure tensile. Further, the deposition of platinum, by sputtering, on top of PZT is compressive. Whereas, the thermal evaporation of chrome/gold, as a top electrode structure on the same PZT structure, is tensile.

The results of the stressed overlayer gave some interesting qualitative findings. Only the titanium/platinum electrode previously processed with PZT produced any delamination as a direct result of the stressed overlayer film. The titanium/platinum bottom electrode pairing and the chrome/gold top electrode pairing were unaffected by the application of a stressed overlayer of platinum. The platinum top electrode was unaffected by the stressed overlayer in that it did not blister in any way but was weakened to such an extent that it peeled when the tape holding it to the sample bed was removed. This occurred for all of the platinum samples irrespective of stressed overlayer thickness.

The qualitative conclusions from the stressed overlayer method are that the titanium/platinum electrode previously processed with PZT has the poorest adhesion qualities, with the platinum electrode deposited on top of PZT being the next poorest. Therefore, in terms of adhesion the top electrode pairing of chrome/gold is preferable to platinum.

In quantitative terms 453nm of platinum producing a stress of 9.85MPa does not produce any delamination in any of the samples. However 906nm of platinum with a stress of 5.81MPa produces delamination, in the form of blisters and some telephone chord-like structures, on the titanium/platinum structure with PZT and etch-back, but not in any of the other samples. Therefore, quantitatively, the weakest electrode structure is the titanium/platinum structure with PZT and etch-back.

An attempt to calculate the work of fracture was conducted using analysis of an almost perfectly circular blister and applying the measurements to a model for a straight-straight buckle of uniform width and height with measurements taken through the centre. In addition, the work of fracture was also calculated using the stresses generated from a Stoney derived one dimensional beam model. This gave an interfacial fracture energy of 1.47 J/m^2 for 108nm of titanium/platinum when subjected to PZT and etch-back. In comparison, Moody et al.(Moody et al., 2007) quote a figure of 41 J/m^2 for the work of adhesion for their stressed overlayer test on SiO_2/Ti 17nm/Pt. However, in all stressed overlayer tests the results are dependent on the mode mixity of stresses (normal to shear) for the fracture induced. In addition, we are dealing with a unique circumstance in that the titanium/platinum layer has been subjected to extrinsic stresses caused by the CSD process with PZT.

5.5 Summary of Conclusions

LNO as a top layer electrode does not look promising by the CSD route, as it stands. However, with a newer sol, suitable cleaning and rapid thermal annealing there may be some promise in the method.

Ruthenium oxide represents a promising material as the deposition method available works on PZT and the results are known to be conductive.

In terms of the adhesion methods under evaluation, pull testing and using a stressed overlayer produced directly useful qualitative results. These gave indication that the bi-material titanium/platinum electrode structure in itself, is well adhered. However, the titanium/platinum bottom electrode structure with PZT and etch-back is self evidently the weakest electrode structure of the samples tested, confirming the anecdotal evidence that it is weakened by the CSD process with PZT. However, in addition to the thermal impact of the CSD process the adhesion qualities of the lower electrode are further undermined by lead diffusion, which means that a more suitable barrier layer needs to be found.

The ranking of the top layer electrodes is clear, in that chrome/gold is preferable over platinum in adhesion terms. Additionally, all of the evidence in relation to platinum indicates that it requires an adhesive layer.

The stressed overlayer technique, in particular offers some real promise in finding the work of fracture for materials. If the mixity of stress is more normal than shear then the value for the work of fracture is potentially one of the closest measures possible for the true work of adhesion.

5.6 Further Work

In terms of the adhesion of the present bottom electrode structure, increasing the titanium or platinum thickness should be investigated. This would be relatively straightforward in that the first concern would be titanium hillock formation and diffusion and these are readily analysed with XPS and depth profiling.

In order to reduce the thermal impact of PZT by CSD it would be useful to increase the individual layer thickness and investigate methods for reducing processing temperatures.

Other investigations could be conducted to see the effects of processing on the surface roughness and grain size and whether this has any impact on adhesion.

In terms of conductive oxides more research is required to determine suitable materials to combine with PZT. Inexorably linked to this, is the cleanliness of the surface and the cleaning regime required for successful deposition.

The stressed overlayer shows rich potential in giving the work of fracture. However, the models associated with various types of buckling from compressive stresses should be investigated and developed so that failure structures can be correctly assessed. In addition, tensile stresses could be used in conjunction with edge peeling models. This could then be used in conjunction with chromium on the Nordiko sputtering system which is very stressy and goes down tensile.

A further suggestion would be the inclusion of a critical load module for the nanoindenter which may give the means for investigating adhesion in thin film structures. Particularly with respect to the investigation of small scale electrode patterns which are directly affected by poling, which is an intrinsic requirement in the use of ferroelectric materials.

Finally, it would be instructive for future work to investigate the impact on adhesion of varying the size and shape of the electrode patterns.

REFERENCES

Bagchi, A. and Evans, A. G. (1996), "Measurements of the debond energy for thin metallization lines on dielectrics", *Thin Solid Films,* vol. 286, no. 1-2, pp. 203-212.

Bagchi, A., Lucas, G. E., Suo, Z. and Evans, A. G. (1994), "A new procedure for measuring the decohesion energy for thin ductile films on substrates", *J.Mater.Res,* vol. 9, no. 7, pp. 1734.

Cheng, J. G., Gabl, R., Pitzer, D., Primig, R., Schreiter, M. and Wersing, W. (2003), "Chemical Solution Deposition of Columnar-Grained Metallic Lanthanum Nitrate Thin Films", *Journal of the American Ceramic Society,* vol. 86, no. 10, pp. 1786-1788.

Cordill, M. J., Bahr, D. F., Moody, N. R. and Gerberich, W. W. (2007), "Adhesion measurements using telephone cord buckles", *Materials Science & Engineering A,* vol. 443, no. 1-2, pp. 150-155.

Franssila, S. (2004), "Introduction to Microfabrication", in Wiley, pp 81-82.

Freund, L. B. and Suresh, S. (2003a), "Thin Film Materials: Stress, Defect Formation, and Surface Evolution", in Cambridge University Press, pp. 60-61.

Freund, L. B. and Suresh, S. (2003b), "Thin Film Materials: Stress, Defect Formation, and Surface Evolution", in Cambridge University Press, pp. 6-9.

Freund, L. B. and Suresh, S. (2003c), "Thin Film Materials: Stress, Defect Formation, and Surface Evolution", in Cambridge University Press, pp. 87-91.

Gerberich, W. W. and Cordill, M. J. (2006), "Physics of adhesion", *REPORTS ON PROGRESS IN PHYSICS,* vol. 69, no. 7, pp. 2173.

Gkotsis, P., Kirby, P. B., Saharil, F., Oberhammer, J. and Stemme, G. (2007), "Thin film crystal growth template removal: Application to stress reduction in lead zirconate titanate microstructures", *Applied Physics Letters,* vol. 91, pp. 163504.

Guerre, R., Drechsler, U., Jubin, D. and Despont, M. (2008), "Selective Transfer Technology for Microdevice Distribution", *Microelectromechanical Systems, Journal of,* vol. 17, no. 1, pp. 157-165.

Guerre, R., Drechsler, U., Jubin, D. and Despont, M. (2007), "CMOS-Compatible Wafer-Level Microdevice-Distribution Technology", *Solid-State Sensors, Actuators and Microsystems Conference, 2007.TRANSDUCERS 2007.International,* , pp. 2087-2090.

Impey. (2007-2008), *Nanomechanical Testing: Scanning Probe Technologies* (unpublished Microsystems and Nanotechnology course notes), SAS, Cranfield University.

Izyumskaya, N. (2007a), "Processing, Structure, Properties, and Applications of PZT Thin Films", *Critical Reviews in Solid State and Materials Sciences,* vol. 32, no. 3, pp. 115-118.

Izyumskaya, N. (2007b), "Processing, Structure, Properties, and Applications of PZT Thin Films", *Critical Reviews in Solid State and Materials Sciences,* vol. 32, no. 3, pp. 125-126.

Izyumskaya, N., Alivov, Y. I., Cho, S. J., Morko, H., Lee, H. and Kang, Y. S. (2007), "Processing, Structure, Properties, and Applications of PZT Thin Films", *Critical Reviews in Solid State and Materials Sciences,* vol. 32, no. 3, pp. 127.

Kim, D. C. and Lee, W. J. (2002), "Effect of $LaNiO_3$ Top Electrode on the Resistance of Pb (Zr, Ti) O_3 ferroelectric capacitor to hydrogen damage and fatigue", *Jpn.J.Appl.Phys., Part 1,* vol. 41, no. 3, pp. 1470-1476.

Kim, J., Kim, K. S. and Kim, Y. H. (1989), "Mechanical effects in peel adhesion test", *Journal of Adhesion Science and Technology,* vol. 3, no. 1, pp. 175-187.

Kinbara, A., Kusano, E., Kamiya, T., Kondo, I. and Takenaka, O. (1998), "Evaluation of adhesion strength of Ti films on Si (100) by the internal stress method", *Thin Solid Films,* vol. 317, no. 1-2, pp. 165-168.

Lee, A., Clemens, B. M. and Nix, W. D. (2004), "Stress induced delamination methods for the study of adhesion of Pt thin films to Si", *Acta Materialia,* vol. 52, no. 7, pp. 2081-2093.

Lee, H. C., Park, J. H., Park, J. Y., Nam, H. J. and Bu, J. U. (2005), "Design, fabrication and RF performances of two different types of piezoelectrically actuated Ohmic MEMS switches", *Journal of Micromechanics and Microengineering,* vol. 15, no. 11, pp. 2098-2104.

Lim W.T., Cho K.R., Lee C.H. (1999), "Structural and electrical properties of rf-sputtered RuO_2 films having different conditions of preparation", *Thin Solid Films*, 348 (1), pp. 56-62.

Madou, M. J. (1997), *Fundamentals of microfabrication,* CRC Press Boca Raton, Fla.

Mittal, K. L. (1976), "Adhesion Measurement of Thin Films", *ElectroComponent Science and Technology*, vol. 3, no. 1, pp. 26.

Miyazaki, H., Goto, T., Miwa, Y., Ohno, T., Suzuki, H., Ota, T. and Takahashi, M. (2004), "Preparation and evaluation of $LaNiO_3$ thin film electrode with chemical solution deposition", *Journal of the European Ceramic Society,* vol. 24, no. 6, pp. 1005-1008.

Modi, M. B. and Sitaraman, S. K. (2004), "Interfacial fracture toughness measurement for thin film interfaces", *Engineering Fracture Mechanics,* vol. 71, no. 9-10, pp. 1219-1234.

Moody, N. R., Adams, D. P., Volinsky, A. A., Kriese, M. D. and Gerberich, W. W. (2000), "Annealing Effects on Interfacial Fracture of Gold-Chromium Films in Hybrid Microcircuits", *Materials Research Society Symposium Proceedings,* vol. 586, pp. 195-206.

Moody, N. R., Kennedy, M. S. and Bahr, D. F. (2007), *Reliability of materials in MEMS: residual stress and adhesion in a micro power generation system.* , SAND2007-6070, Sandia National Laboratories.

Muralt, P. (2000), "PZT thin films for microsensors and actuators: Where do we stand?", *IEEE transactions on ultrasonics, ferroelectrics, and frequency control,* vol. 47, no. 4, pp. 903-915.

Nam, H. J., Choi, D. K. and Lee, W. J. (2000), "Formation of hillocks in Pt/Ti electrodes and their effects on short phenomena of PZT films deposited by reactive sputtering", *Thin Solid Films,* vol. 371, no. 1-2, pp. 264-271.

Sama, N., Herdier, R., Jenkins, D., Soyer, C., Remiens, D., Detalle, M. and Bouregba, R. (2008), "On the influence of the top and bottom electrodes—A comparative study between Pt and LNO electrodes for PZT thin films", *Journal of Crystal Growth,* vol. 310, no. 14, pp. 3299-3302.

Steinmann, P., Tardy, Y. and Hintermann, H. E. (1987), "Adhesion Testing by the Scratch Test Method: the Influence of Intrinsic and Extrinsic Parameters on the Critical Load", *Thin Solid Films,* vol. 154, no. 1, pp. 333-349.

Stoney, G. G. (1909), "The Tension of Metallic Films Deposited by Electrolysis", *Proceedings of the Royal Society of London.Series A, Containing Papers of a Mathematical and Physical Character,* vol. 82, no. 553, pp. 172-175.

Valdes, L. B. (1954), "Resistivity Measurements on Germanium for Transistors", *Proceedings of the IRE,* vol. 42, no. 2, pp. 420-427.

Wilson, S. A., Jourdain, R. P. J., Zhang, Q., Dorey, R. A., Bowen, C. R., Willander, M., Wahab, Q. U., Willander, M., Al-hilli, S. M. and Nur, O. (2007a), "New materials for micro-scale sensors and actuators An engineering review", *Materials Science & Engineering R,* vol. 56, no. 1-6, pp. 7.

Wilson, S. A., Jourdain, R. P. J., Zhang, Q., Dorey, R. A., Bowen, C. R., Willander, M., Wahab, Q. U., Willander, M., Al-hilli, S. M. and Nur, O. (2007b), "New materials for micro-scale sensors and actuators An engineering review", *Materials Science & Engineering R,* vol. 56, no. 1-6, pp. 9-10.

Yuh, H. K., Yoon, E., Lee, Y. T., Park, Y. W. and Lee, S. I. (2002), "Effects of Pb/Pt Top Electrode on Hydrogen-Induced Degradation in Pb (Zr, Ti) O_3", *Jpn. J. Appl. Phys.,* vol. 41, no. 1, pp. pp. 42-46.

Zheng, J. and Sitaraman, S. K. (2007), "Fixtureless superlayer-driven delamination test for nanoscale thin-film interfaces", *Thin Solid Films,* vol. 515, no. 11, pp. 4709-4716.

Appendices

Appendix A

Table A1 Peak Comparer and Percentage Quantities

Peak		Area	ASF	Atoms	At%		
Pt	1	214677	4.4	48790	12.8	Pt	32.9
Pt	2	103951	4.4	23625	6.2		0.0
Pt	3	182575	4.4	41494	10.9		0.0
Pt	4	51572	4.4	11721	3.1		0.0
Pb	1	21566	3.85	5602	1.5	Pb	1.9
Pb	2	5653	3.85	1468	0.4		0.0
C	1	34158	0.25	136632	35.8	C	43.8
C	2	7671	0.25	30684	8.030265		0.0
O	1	14889	0.66	22559	5.903907	O	21.5
O	2	33818	0.66	51239	13.40979		0.0
O	3	5471	0.66	8289	2.169405		0.0

Appendix B

Table A2 Four point probe measurements for Chrome/Gold Reference

Current / mA	Voltage/ mV
0.1	0.006
0.2	0.012
0.3	0.018
0.4	0.025
0.5	0.031
0.6	0.037
0.7	0.044
0.8	0.050
0.9	0.056
1.0	0.063
2	0.126
3	0.189
4	0.253
5	0.317
6	0.380
7	0.444

Figure A1 Graph of Chrome/Gold Voltage/Current Measurements

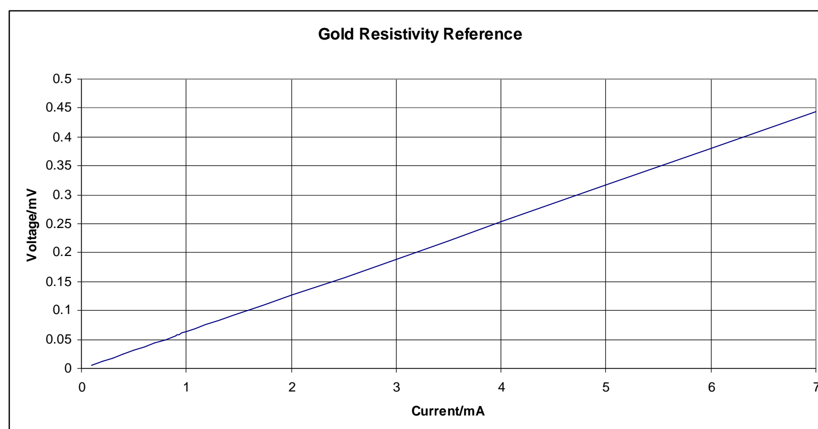

Table A3 Four Point Probe Measurements for Ruthenium Oxide on Glass Slides

Current / mA	Sample 1 Before Anneal Voltage/ mV	Sample 1 Annealed at 450°C Voltage/ mV	Sample 2 Before Anneal Voltage/ mV	Sample 2 Annealed at 550°C Voltage/ mV
0.1	0.070	0.047	0.065	0.025
0.2	0.145	0.094	0.131	0.048
0.3	0.218	0.14	0.196	0.072
0.4	0.290	0.187	0.262	0.096
0.5	0.363	0.233	0.328	0.119
0.6	0.436	0.280	0.394	0.143
0.7	0.509	0.327	0.460	0.167
0.8	0.581	0.373	0.526	0.190
0.9	0.654	0.420	0.592	0.214
1.0	0.726	0.466	0.658	0.238
2	1.454	0.932	1.318	0.475
3	2.180	1.398	1.977	0.713
4	2.900	1.864	2.637	0.950
5	3.630	2.329	3.296	1.188
6	4.360	2.795	3.956	1.426

The effect of annealing at 450°C on the voltage and current relationship for Sample 1 is shown below.

Figure A2 Effect of Annealing at 450°C on V/I Relationship

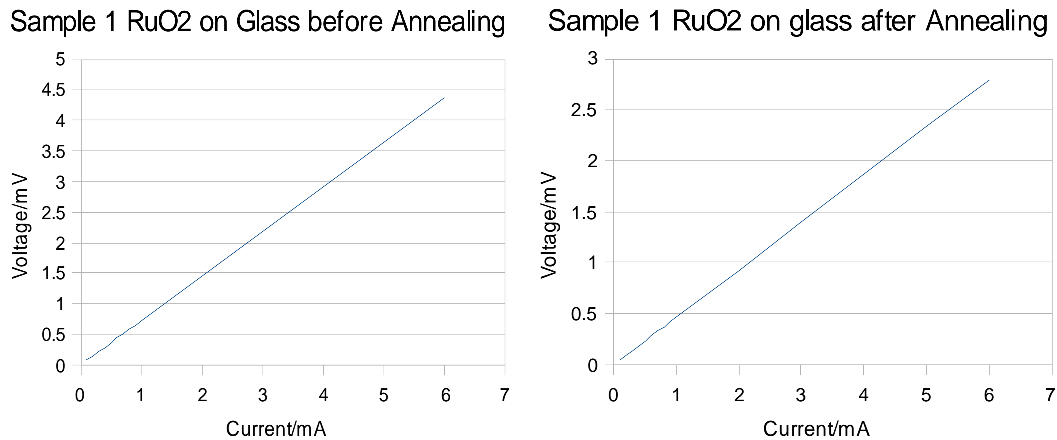

The effect of annealing at 550°C on the voltage and current relationship for Sample 2 is shown below.

Figure A3 Effect of Annealing at 550°C on V/I Relationship